



---

The University of Reading

# GRAVITY WAVES IN MULTILAYER SYSTEMS

Jemma Shipton

supervised by Dr Maarten Ambaum and funded by NERC

*Submitted to the Department of Mathematics, University of Reading, in partial fulfilment of the requirements for the Degree of Master of Science.*

*I confirm that this is my own work and the use of all material from other sources has been properly and fully acknowledged.*

## **Acknowledgements**

I would like to thank my supervisor, Maarten Ambaum, for his help and encouragement throughout this project. I am extremely grateful for his guidance and useful suggestions.

Thanks also to my family for their support, and to all the other M.Sc. students for making this year so enjoyable. Special thanks to Dan for cooking me numerous dinners and picking me up from the department whenever I've worked here after dark.

This dissertation and my year of study at Reading University has been financed by the National Environmental Research Council.

## **Abstract**

The generation of gravity waves by topography is examined in this study. These waves are important in the atmosphere on all scales. Their interaction with the mean flow has implications for global atmospheric circulation. They also feature prominently in localised weather in mountainous or hilly regions.

The equations of motion for an homogeneous layer of fluid flowing over a symmetric, one dimensional, isolated mountain are studied and it is found that there is a critical mountain height above which the solution becomes discontinuous. An expression for this critical height is derived.

A numerical model is developed to solve the nonlinear shallow water equations in a homogeneous layer and the results it produces are compared with established results.

The theory of stratified flow is presented. The effect of approximating continuous vertical profiles of buoyancy frequency and velocity by a finite set of discrete layers is discussed and this multilayer approach is further investigated with the aid of an extension of the single layer numerical model written by the author. The results are compared to established solutions and suggestions are put forward for further work.

# Contents

<b>1</b>	<b>Introduction</b>	<b>1</b>
1.1	Gravity wave formation . . . . .	1
1.2	Meteorological applications . . . . .	2
1.2.1	Lee waves . . . . .	3
1.2.2	Gravity wave drag . . . . .	6
1.3	Modelling atmospheric gravity waves . . . . .	7
1.4	Aims . . . . .	7
<b>2</b>	<b>The flow of a single homogeneous layer</b>	<b>9</b>
2.1	The basic equations . . . . .	9
2.2	Linear hydrostatic flow . . . . .	11
2.3	Nonlinear hydrostatic flow . . . . .	12
2.3.1	The program . . . . .	16
2.3.2	Sensitivity to parameters . . . . .	19
2.3.3	Results . . . . .	20
<b>3</b>	<b>Stratified flow</b>	<b>27</b>
3.1	Basic equations . . . . .	27
3.2	Energetics . . . . .	29
3.3	Wind stress . . . . .	31
3.4	Wave reflection, trapping and resonance . . . . .	32
3.5	The hydrostatic approximation . . . . .	34

<b>4</b>	<b>The multilayer model</b>	<b>36</b>
4.1	Multilayer equations . . . . .	36
4.2	Multilayer program . . . . .	38
4.2.1	Sensitivity to parameters . . . . .	40
4.3	Results . . . . .	40
4.3.1	Two layer flow . . . . .	40
4.3.2	Partial reflection . . . . .	41
4.3.3	Variation of buoyancy frequency . . . . .	44
4.3.4	Vertical wind profile . . . . .	46
<b>5</b>	<b>Conclusions</b>	<b>48</b>
5.1	Evaluation of the multilayer model . . . . .	48
5.1.1	Resolution . . . . .	48
5.1.2	The sponge layer . . . . .	49
5.1.3	The hydrostatic approximation . . . . .	49
5.2	Further work . . . . .	49
5.2.1	Layers with uniform density and vorticity . . . . .	50
5.2.2	Rotational effects . . . . .	50
5.2.3	Extension to more dimensions . . . . .	50

# List of Figures

1.1	A lenticular cloud. . . . .	4
1.2	A series of lenticular clouds. . . . .	5
1.3	Lee waves in a stratified flow. . . . .	6
2.1	Single layer diagram . . . . .	11
2.2	Example of the linear solution for flow over an obstacle. . . . .	12
2.3	x-t diagram showing the linear solution for subcritical flow over an obstacle. . .	13
2.4	x-t diagram showing the linear solution for supercritical flow over an obstacle. .	13
2.5	Shock wave formation . . . . .	14
2.6	$g(D, F_0, H)$ for $F_0 = 0.5$ . . . . .	17
2.7	$g(D, F_0, H)$ for $F_0 = 1.5$ . . . . .	17
2.8	The non-dimensional maximum height of the mountain, $H_{max}$ , as a function of the initial Froude number, $F_0^2$ . . . . .	18
2.9	Nonlinear subcritical flow. . . . .	22
2.10	Nonlinear supercritical flow. . . . .	22
2.11	Nonlinear flow with shocks (1) . . . . .	23
2.12	Nonlinear flow with shocks (2) . . . . .	23
2.13	x-t diagram of the numerical solution (blue) compared to the exact linear solu- tion (red) for the case where $h_{max} \ll h_{crit}$ . . . . .	25
2.14	x-t diagram of the numerical solution (blue) compared to the exact linear solu- tion (red) for the case where $h_{max} < h_{crit}$ . . . . .	25
2.15	x-t diagram of the numerical solution (blue) compared to the exact linear solu- tion (red) for the case where $h_{max} \sim h_{crit}$ . . . . .	26

4.1	Multilayer diagram . . . . .	37
4.2	Diagram of the multilayer program. . . . .	39
4.3	Two layer flow . . . . .	41
4.4	Numerical result from the multilayer model for the atmospheric profile detailed in equations (4.3.2),(4.3.2) and (4.3.2) . . . . .	43
4.5	Linear streamline pattern for flow past a bell shaped mountain. From Klemp and Lilly (1975) . . . . .	43
4.6	$d_i(x)$ for $m = 0.001m^{-1}$ . . . . .	44
4.7	$d_i(x)$ for $m = 0.002m^{-1}$ . . . . .	45
4.8	Location of maximum wave amplitudes. . . . .	45
4.9	Initial vertical velocity profile, $U(z)$ . . . . .	46
4.10	A comparison of $d_i(x)$ in the case where $U(z)$ is as given in figure 4.9 (blue), to the case where $U = 10ms^{-1}$ is constant with height (red). . . . .	47
4.11	A plot of the difference between the two cases shown in figure 4.10. . . . .	47

# Chapter 1

## Introduction

### 1.1 Gravity wave formation

Atmospheric gravity waves are produced when a disturbance causes the air to be displaced from its equilibrium position. Consider an incompressible atmosphere in equilibrium and a fluid parcel of density  $\rho(z_0)$  at height  $z_0$ . If the parcel is displaced a small distance  $\delta z$  then, assuming it remains intact and does not mix with its surroundings, the parcel will experience a buoyancy force  $\mathbf{F}_b$  which is given by Archimedes' Law:

$$\mathbf{F}_b = -gv(\rho(z_0) - \rho(z_0 + \delta z))\hat{z}, \quad (1.1)$$

where  $g$  is the acceleration due to gravity,  $v$  is the volume of displaced air which is equal to the volume of the parcel, and  $\rho(z_0 + \delta z)$  is the density of the air displaced by the parcel. By Newton's second law of motion

$$\frac{d^2(\delta z)}{dt^2} = -g \frac{\rho(z_0) - \rho(z_0 + \delta z)}{\rho(z_0)}. \quad (1.2)$$

Expanding  $\rho(z_0 + \delta z)$  as a Taylor series gives

$$\rho(z_0 + \delta z) = \rho(z_0) + \left. \frac{\partial \rho}{\partial z} \right|_{z=z_0} \delta z + \dots \quad (1.3)$$

Using this, equation (4.3.2) becomes

$$\frac{d^2 \delta z}{dt^2} = \frac{g}{\rho} \frac{\partial \rho}{\partial z} \delta z. \quad (1.4)$$

This is the equation for simple harmonic motion. It has the solution

$$\delta z(t) = Ae^{iNt} + Be^{-iNt}, \quad (1.5)$$

where

$$N^2 = -\frac{g}{\rho} \frac{\partial \rho}{\partial z}. \quad (1.6)$$

$N$  is therefore a measure of the stratification of the fluid. For  $\partial \rho / \partial z > 0$ , the perturbation grows unboundedly and the solution is unstable. If  $\partial \rho / \partial z < 0$ ,  $N$  is real and the air parcel oscillates with frequency  $N$ . Under these conditions the atmosphere is said to be stably stratified. Gravity waves can have any frequency between 0 and  $N$  since the displacements of air parcels within the wave can be at an angle  $\alpha$  to the horizontal. In this case the distance  $\delta z$  in (1.4) is replaced by  $\sin^2 \alpha \delta s$  and  $N$  becomes  $N' = N \sin \alpha$ . Typical values of  $N$  are  $0.01 s^{-1}$  in the troposphere and  $0.017 s^{-1}$  in the stratosphere (Gill, 1982).

So far we have assumed the atmosphere to be incompressible so that density is conserved. A more accurate assumption would be that the atmosphere is adiabatic. In this case it is the potential temperature,  $\theta = T(p_0/p)^k$ , where  $p_0$  is the surface pressure, that is conserved. However, to a good approximation, the above analysis still holds.

We have seen that disturbances in a fluid can lead to the formation of gravity waves. In the atmosphere these disturbances can be caused by the effects of orography and also by convection and the resulting release of latent heat (Nappo, 2002). In this study the source of the disturbance will be a one dimensional, symmetric, isolated mountain.

## 1.2 Meteorological applications

Operational forecast models solve an approximation to the full governing equations that filters out gravity waves. This is necessary because the resolution required to explicitly include them would result in an unreasonable execution time. However, the effects of these waves are far from negligible. Gravity waves are important on all scales in the atmosphere. On the large scale gravity wave drag can

slow the mean flow. On a localised scale, gravity waves are associated with lenticular cloud formations and downslope winds such as the Fohn in the Alps and the Chinook in the Rocky mountains. A particularly severe windstorm that has been extensively studied is that which occurred in Boulder, Colorado in January 1969 where wind gusts measured up to 130mph. The strong wind speeds have been attributed to partial reflection of gravity waves from a critical layer aloft. Such layers will be studied in section 4.3.2. A better understanding of the formation and propagation of these waves will lead to better parameterisation of their effects in global circulation models.

In the next two sections we briefly summarise the local and global effects of gravity waves.

### 1.2.1 Lee waves

Gravity waves are also the source of some spectacular cloud formations such as those shown in figure 1.1. These lenticular clouds are formed in the lee of mountains. As the air is forced up over the mountain it cools and may reach the dew point temperature in which case the water vapour it contains will start to condense and form droplets. As the air descends again on the other side of the mountain it warms and the water droplets vaporise. However, the continual motion of the airstream means that the water droplets are constantly being replaced so an observer will see a stationary cloud attached to the mountain - only a pilot will experience the dangerous winds within it. If the conditions are such that a standing pattern of lee waves is created, a series of lenticular clouds can form downstream (see figure 1.2).

Due to the stationary appearance of the cloud formations associated with Lee waves, their importance in the atmosphere was not realised until the experiences of gliders and pilots began to reveal the existence of unexplained localised currents near topography. Queney (1948) details the observations that needed explaining:

- strong ascending currents, often to a great height, especially on the upwind side of mountain ranges,



Figure 1.1: A lenticular cloud, courtesy of Jay Shafer, <http://vortex.plymouth.edu/lenticular3.html>.

- stationary lenticular clouds and cloudless areas in stratocumulous sheets,
- periodical nature of current above large mountain ranges,
- stationary pressure ridges (on crest) and troughs (on lee side),
- formation of intense narrow winds.

The effects can, to a great extent, be explained by the linear theory of internal gravity waves in a stratified fluid. There are two factors that control the development of lee waves: the dimensions of the topography and the characteristics of the airstream. Both must satisfy certain conditions for lee waves to exist and it has been shown (Corby and Wallington, 1956) that the largest amplitude waves occur when the optimum conditions are satisfied by only a small margin.

Scorer (1949) shows that if the airstream satisfies the condition that

$$L^2 = \frac{N^2}{U^2} - \frac{1}{U} \frac{d^2U}{dz^2} \quad (1.7)$$

decreases upwards at a sufficient rate, lee waves will form. For a system consisting



Figure 1.2: A series of lenticular clouds, courtesy of Gary Schultz, <http://www.williwaw.com/2001-SEP.html>.

of two layers of constant  $L^2$ , the condition

$$L_1^2 - L_2^2 > \frac{\pi}{4h^2}, \quad (1.8)$$

where  $h$  is the depth of the lower layer, must be satisfied for lee waves to form. Sawyer (1960) shows that, although Scorer's condition is sufficient, it is not necessary and there are other airstream properties that can give rise to lee waves. He demonstrates this by considering the case of a two layer atmosphere in which the top layer is significantly more stable than the lower layer and his numerical results are shown in figure 1.3.

Queney (1948) investigates the conditions of the dimensions of the topography. He shows that, for an airstream with uniform stratification and windspeed, the atmospheric response to a mountain range depends on the half-width  $a$  of the range. The main situation of interest to us is that where  $a \sim U/N$ , where  $U$  and  $N$  are the velocity and buoyancy frequency of the airstream. In this case a system of gravity waves with wavelength  $\lambda = 2\pi U/N$  develops in the lee of the mountain. Queney (1948) considers two other values of  $a$  that produce either in-

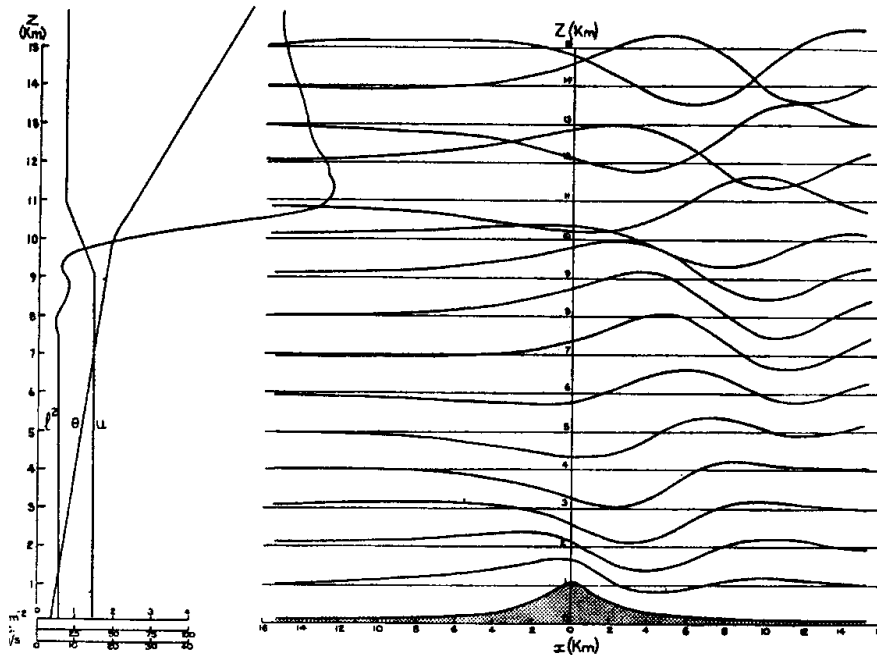


Figure 1.3: Displacement of streamlines computed for an airstream with the vertical profiles of  $L^2$ ,  $U$  and  $N$  plotted on the left. A train of rapidly decaying lee waves develops despite the fact that the  $L^2$  profile does not satisfy Scorer's condition. After Sawyer (1960)

ertia gravity waves or Rossby waves but we are not concerned with the effects of rotation here.

## 1.2.2 Gravity wave drag

On a larger scale, gravity waves transport energy and momentum which they exchange with the mean flow. This can, due to wind stress over terrain, slow the atmospheric flow at a rate of  $5ms^{-1}day^{-1}$  (Nappo, 2002). The energy or momentum carried by the waves will not be deposited unless the wave breaks or is dissipated. Such dissipation can occur at critical levels in the atmosphere where the wind speed is equal to the speed of the waves. This will be investigated in section 3.3.

### 1.3 Modelling atmospheric gravity waves

There are many ways of approaching the study of atmospheric gravity waves, all of which involve making some approximations either to the topography, to the airstream properties or to the governing equations. Exact solutions to the nonlinear wave equation are only possible under specific conditions, for example, that the flow has constant density or buoyancy frequency. Under these constraints the governing equation becomes linear but the lower boundary condition remains nonlinear. This is known as Long's model. Some progress has been made towards finding exact solutions for some idealized mountain shapes (Baines (1995) and references therein) but these kind of shapes are not found in practice. Another approach is to assume that any perturbations are small and therefore terms involving products of perturbations can be neglected. These linearised equations offer a method that imposes less restriction on the types of airstream studied and give an insight into the properties of the flow. However, the linear theory is only valid for small amplitude waves and, since the wave momentum and energy fluxes are proportional to the square of its amplitude, it is the large amplitude waves that are of interest in the atmosphere.

### 1.4 Aims

The aim of this study is to investigate the vertical propagation of gravity waves created by flow over a single isolated mountain. We have seen that this process is important in a meteorological context due to the energy and momentum they transport. Our attention will be restricted to situations where the effects of rotation are negligible. We will be using a numerical model to simulate some real flows. This model will approximate continuous atmospheric profiles by a finite set of discrete, homogeneous layers. The nonlinear, hydrostatic governing equations are then solved in each layer with the appropriate matching conditions at the interface. We hope to verify some published results produced using linear models and to investigate some of the effects of nonlinearity on the flow.

In chapter 2 we will examine the flow of a single, homogeneous layer over an obstacle. We will discuss the theory of such a flow and present some results from the one layer model.

Chapter 3 develops the theory of continuously stratified flow. We briefly discuss the energy, momentum and wind stress associated with gravity waves. Wave reflection and trapping will also be investigated.

In chapter 4 we analyse the flow of a multilayer fluid. The governing equations are derived and solved numerically. The multilayer program is tested and the results discussed.

Chapter 5 presents the conclusions and outlines the possibilities for further work.

# Chapter 2

## The flow of a single homogeneous layer

### 2.1 The basic equations

Consider a layer of 2-dimensional, incompressible, homogeneous fluid with a free surface flowing over an isolated mountain. The equations of motion for such a fluid with density  $\rho$  and pressure  $p$  are

$$\frac{D\mathbf{u}}{Dt} = -\frac{1}{\rho}\nabla p - g\hat{\mathbf{z}}, \quad (2.1)$$

$$\nabla \cdot \mathbf{u} = 0, \quad (2.2)$$

where  $\mathbf{u} = (u, w)$  is the fluid velocity with components in the Cartesian  $(x, z)$  directions and  $\hat{\mathbf{z}}$  is the vertical unit vector. At its lower boundary the fluid encounters topography  $z = h(x)$  and the condition that there can be no flow through this surface gives

$$w = \mathbf{u} \cdot \nabla h \text{ on } z = h(x). \quad (2.3)$$

The fluid has an upper free surface with mean level  $z = \bar{d}$  and displacement  $\eta(x)$  as shown in figure 2.1. Assuming the density of any fluid above this surface to be negligible and taking the pressure there to be zero we have

$$w = \frac{D\eta}{Dt} \text{ on } z = \bar{d} + \eta. \quad (2.4)$$

Assuming the vertical accelerations to be small compared to gravity, we can apply the hydrostatic approximation

$$-\frac{1}{\rho}p_z - g = 0. \quad (2.5)$$

Integrating this gives an expression for the pressure

$$p = p_s + \rho g(\bar{d} + \eta - z), \quad (2.6)$$

where  $p_s$  is the pressure at the surface. From this equation we can see that  $p_x$  is independent of  $z$  so if  $\mathbf{u}$  is initially independent of  $z$  it will remain so. Substituting (2.6) into (2.1) gives

$$u_t + uu_x = -g\eta_x. \quad (2.7)$$

This gives us the prognostic equation for the velocity  $u$  within the layer. To obtain the prognostic equation for the surface displacement  $\eta$  we need to integrate (2.2) between  $z = h$  and  $z = \bar{d} + \eta$ :

$$0 = \int_h^{\bar{d}+\eta} (u_x + w_z) dz \quad (2.8)$$

$$= \frac{\partial}{\partial x} \int_h^{\bar{d}+\eta} u dz - u\eta_x + uh_x + [w]_h^{\bar{d}+\eta}. \quad (2.9)$$

From the boundary conditions (2.3) and (2.4), this reduces to

$$\frac{\partial}{\partial x} \int_h^{\bar{d}+\eta} u dz + \frac{\partial \eta}{\partial t} = 0. \quad (2.10)$$

Remembering that, by (2.6),  $\mathbf{u}$  independent of  $z$ , equation (2.10) becomes

$$\eta_t + (du)_x = 0, \quad (2.11)$$

where  $d = \bar{d} + \eta - h$ . So the motion of the layer is described by equations (2.7) and (2.11). These equations are nonlinear and they can be tackled in two ways. The first method, described in the next section, approximates the properties of the flow by assuming any perturbations to the background state to be small. The second method approximates the equations by representing the flow variables on a grid and solving the resulting discrete equations numerically.

## 2.2 Linear hydrostatic flow

Consider a steady one dimensional flow with speed  $U$  approaching an obstacle of small height as shown in figure 2.1.

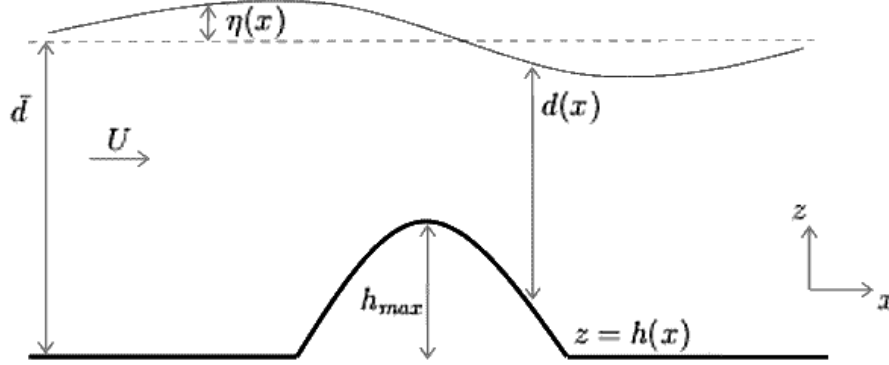


Figure 2.1: Definition diagram for the notation in the single layer case.  $U$  and  $\bar{d}$  are respectively the upstream constant speed and depth,  $\eta(x)$  is the displacement of the free surface and  $h(x)$  is the topography.  $d(x) = \bar{d} + \eta(x) - h(x)$  is the total depth of the fluid layer.

Under these conditions we can set  $u(x) = U + u'(x)$  and assume  $u'(x)$ ,  $\eta(x)$  and  $h(x)$  to be small perturbations. Substituting into (2.7) and (2.11) and linearising gives

$$u'_t + Uu'_x = -g\eta_x, \quad (2.12)$$

$$\eta_t + U\eta_x + \bar{d}u'_x = Uh_x. \quad (2.13)$$

Eliminating  $u'$  leaves

$$\left(\frac{\partial}{\partial t} + U\frac{\partial}{\partial x}\right)^2 \eta - c^2 \frac{\partial^2 \eta}{\partial x^2} = U^2 \frac{\partial^2 h}{\partial x^2}, \quad (2.14)$$

where  $c = \sqrt{g\bar{d}}$  is the wave speed. With initial conditions  $\eta = 0$  and  $\eta_t = 0$ , 2.14 has solution

$$\eta = \frac{F_0^2}{F_0^2 - 1} h(x) - \frac{F_0}{2} \left( \frac{1}{F_0 + 1} h(x - (U + c)t) + \frac{1}{F_0 - 1} h(x - (U - c)t) \right) \quad (2.15)$$

when the initial Froude number  $F_0 = U/c \neq 1$ . This solution, for  $F_0 < 1$  is shown in figure 2.2. It is made up of a steady component over the obstacle and two propagating waves which are functions of the characteristic variables. All three terms have the same form as the obstacle but with different amplitudes which depend solely on the initial conditions.

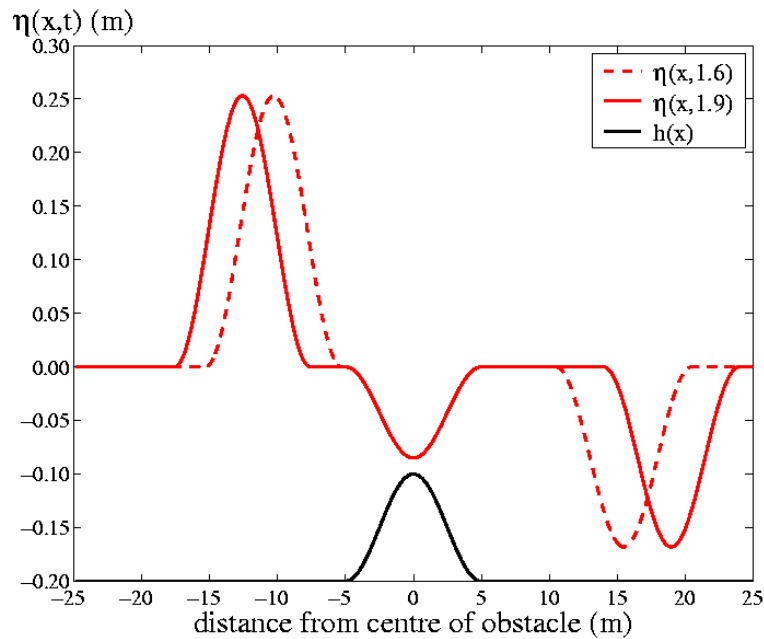


Figure 2.2: Example of the linear solution for flow over an obstacle.

For  $F_0 < 1$  the upstream propagating wave has larger amplitude. The two types of flow are shown in figures 2.3 and 2.4.

### 2.3 Nonlinear hydrostatic flow

The linear equations are only valid for sufficiently small  $h_{max}$ . When  $h_{max}$  does not satisfy this constraint, nonlinear effects become apparent and can even dominate the system. One important nonlinear phenomenon is the hydraulic jump or shock. Although this study will be restricted to cases where there are no shocks, it is important to know the circumstances under which they form so that they can

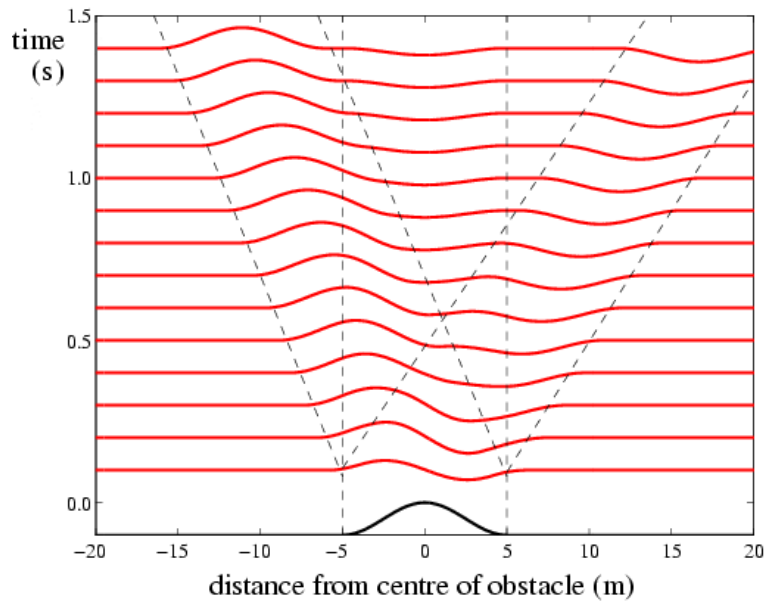


Figure 2.3: x-t diagram showing the linear solution for subcritical flow over an obstacle.

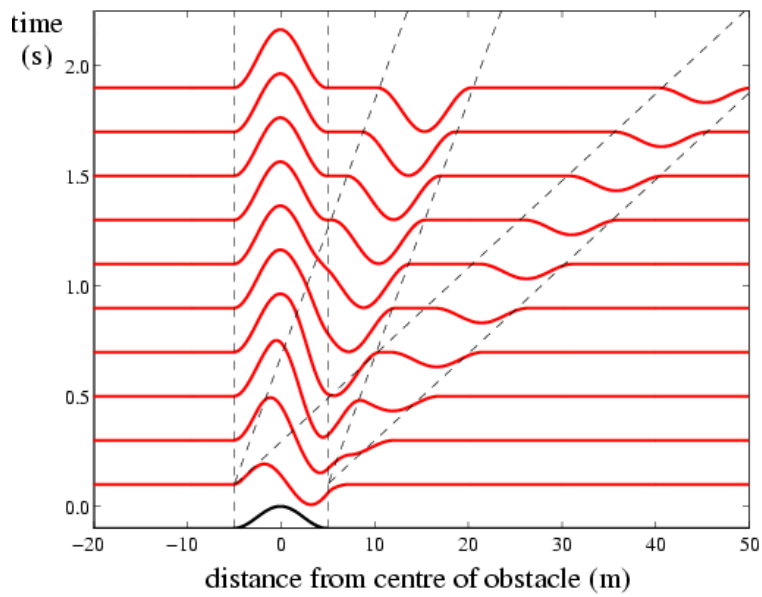


Figure 2.4: x-t diagram showing the linear solution for supercritical flow over an obstacle.

be avoided. Consider the case shown in figure 2.5 where the wave initially has a small amplitude but, as the deeper fluid moves faster, the interface steepens and may become vertical. This is the shock which, if required, can be modelled as a discontinuity. At a shock, the flow changes from supercritical to subcritical or vice-versa and this suggests that the local Froude number at this point must be unity. This is shown to be true later on in this section.

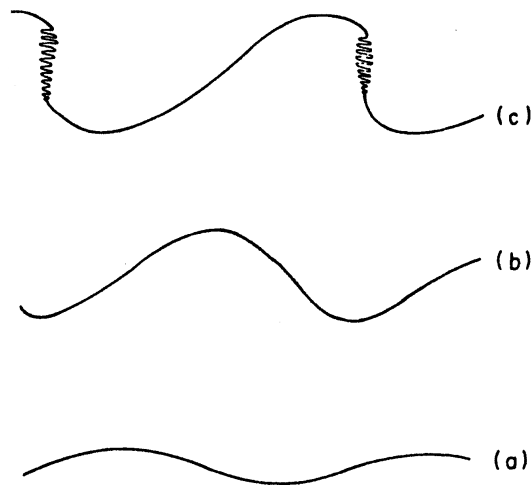


Figure 2.5: This diagram illustrates the formation of a shock wave. The initial wave is that labelled (a). As its amplitude increases the profile steepens until, as in case (c), the wave breaks. Adapted from Andrews and Leovy. (1987).

Following Houghton and Kasahara (1968) we examine the steady state equations in order to derive a condition on the maximum mountain height that will ensure that there are no shocks in the flow. The steady state forms of equations (2.7) and (2.11) are

$$\frac{d}{dx} \left( \frac{1}{2} u^2 + g(d+h) \right) = 0, \tag{2.16}$$

$$\frac{d}{dx} (ud) = 0, \tag{2.17}$$

which, when integrated, give

$$\frac{1}{2}u^2 + g(d+h) = \frac{1}{2}U^2 + g\bar{d}, \quad (2.18)$$

$$ud = U\bar{d}. \quad (2.19)$$

Using (2.19) to eliminate  $u$  from (2.18) gives

$$\frac{1}{2}U^2\frac{\bar{d}^2}{d^2} + g(d+h) = \frac{1}{2}U^2 + g\bar{d}, \quad (2.20)$$

which can be rewritten in terms of the dimensionless variables  $F_0 = U/c$ ,  $D = d/\bar{d}$  and  $H = h/\bar{d}$  as

$$D^3 + \left(H - \frac{1}{2}F_0^2 - 1\right)D^2 + \frac{1}{2}F_0^2 = 0. \quad (2.21)$$

Figure 2.6 shows this polynomial, plotted as a function of  $D$ , for  $F_0 = 0.5$  and three different values of  $H$ . Since  $F_0 < 1$  the fluid will dip over the obstacle so  $d < \bar{d}$  and  $D < 1$  and the root of the polynomial corresponding to the physical solution is that between 0 and 1. Figure 2.7 shows the same polynomial for  $F_0 = 1.5$ . In this case the fluid rises over the obstacle and the root we are interested in is the first which is greater than 1. In both cases, it can be seen that for  $H$  greater than some critical value  $H_{crit}$ , there is no physically meaningful solution. Having demonstrated this graphically we now give a mathematical argument. Defining the function

$$g(D, F_0, H) = D^3 + \left(H - \frac{1}{2}F_0^2 - 1\right)D^2 + \frac{1}{2}F_0^2, \quad (2.22)$$

we see that for there to be a solution to  $g = 0$  for a given height  $H$ , we must have

$$\delta g = \frac{\partial g}{\partial F_0}\delta F_0 + \frac{\partial g}{\partial D}\delta D = 0. \quad (2.23)$$

Except in the trivial case  $D = 1$  which corresponds to the solution for flow over a flat horizontal boundary,  $\partial g/\partial F_0 = F_0(1 - D^2)$  is non-zero. Thus any small change in  $F_0$  must be balanced by a small change in  $D$ . This can only occur if  $\partial g/\partial D \neq 0$ . This condition gives us an equation for the critical depth  $D_{crit}$ . Calculating the partial derivative of  $g$  with respect to  $D$  gives

$$\frac{\partial g}{\partial D} = 3D^2 + 2D\left(H - \frac{1}{2}F_0^2 - 1\right). \quad (2.24)$$

This is zero when

$$D = D_{crit} = -\frac{2}{3}\left(H - \frac{1}{2}F_0^2 - 1\right). \quad (2.25)$$

Imposing the condition  $g(D_{crit}, F_0, H) = 0$  gives

$$D_{crit}^3 = F_0^2. \quad (2.26)$$

So we have found an expression for the critical depth at which  $g = 0$  has no solutions. We now use this to find an equation for the critical mountain height. Rearranging (2.18) gives

$$D^3 = \frac{F_0^2}{F^2}, \quad (2.27)$$

where  $F = u/\sqrt{gd}$ . Comparing this with (2.26), shows that the local Froude number  $F^2$  must be unity at the critical point. Setting  $F^2 = 1$  in (2.26) and substituting this into (2.21) gives, after some rearrangement,

$$H_{crit} = 1 + \frac{1}{2}F_0^2 - \frac{3}{2}F_0^{2/3}. \quad (2.28)$$

This function is plotted in figure 2.8. Long has shown (Long, 1954) that any  $H$  greater than  $H_{crit}$  will cause the solution to become discontinuous, so  $h_{crit} = H_{crit}\bar{d}$  is the maximum height of the mountain for which the flow does not contain shocks. In this study we will restrict our attention to mountains with  $h_{max} < h_{crit}$ , the shaded area in figure 2.8.

The introduction of shocks is not the only effect of using the full nonlinear equations. Some steepening of the waves is still likely even if a shock is not finally formed.

### 2.3.1 The program

The program `single_layer_program.f90` solves equations (2.7) and (2.11) for  $U$ ,  $\bar{d}$  and  $h_{max}$  as input by the user. Since we do not wish to analyse shocks it is not necessary to use a shock fitting or shock capturing method. Instead the program uses a simple leapfrog method which solves

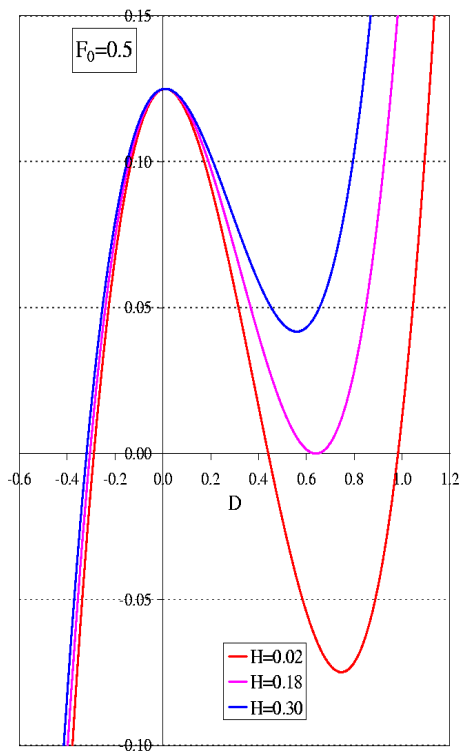


Figure 2.6:  $g(D, F_0, H)$  for  $F_0 = 0.5$ . The red curve has  $H < H_{crit}$  and the blue curve has  $H > H_{crit}$ . The purple curve shows that for  $H = H_{crit}$  there is a double root.

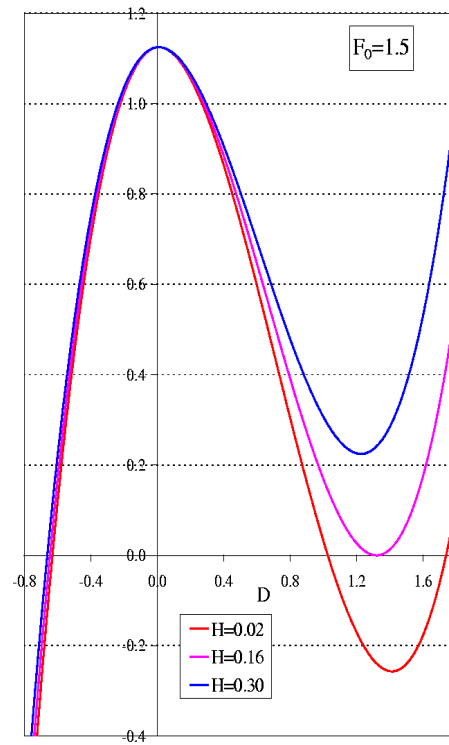


Figure 2.7:  $g(D, F_0, H)$  for  $F_0 = 1.5$ . The red curve has  $H < H_{crit}$  and the blue curve has  $H > H_{crit}$ . The purple curve shows that for  $H = H_{crit}$  there is a double root.

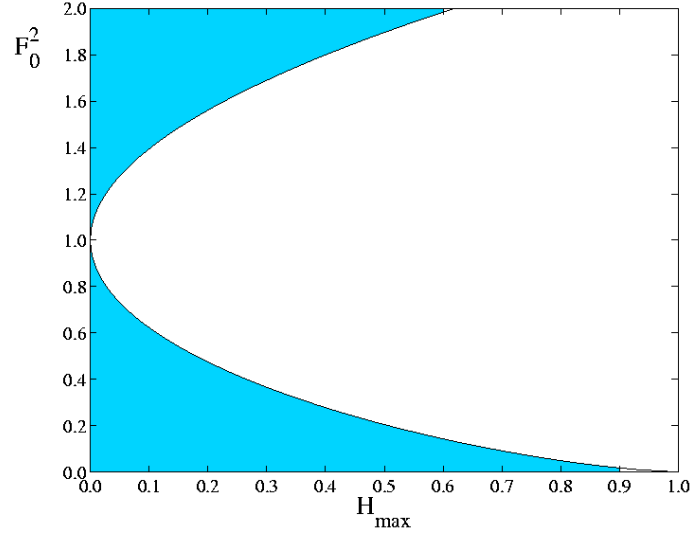


Figure 2.8: The non-dimensional maximum height of the mountain,  $H_{max}$ , as a function of the initial Froude number,  $F_0^2$

$$u_j^{n+1} = u_j^{n-1} - \frac{dt}{dx} \left( F_{j+1}^n - F_{j-1}^n \right), \quad (2.29)$$

$$\eta_j^{n+1} = \eta_j^{n-1} - \frac{dt}{dx} \left( K_{j+1}^n - K_{j-1}^n \right), \quad (2.30)$$

where

$$F_j^n = \frac{1}{2}(u_j^n)^2 + g\eta_j^n, \quad (2.31)$$

$$K_j^n = u_j^n(\bar{d} + \eta_j^n - h_j), \quad (2.32)$$

and  $q_j^n$  denotes the value of variable  $q$  at  $(x_j, t^n)$ . In order to study the steady state solution we require the transient waves to leave the domain. This is easily accomplished by including a wave absorbing, or sponge, layer at the lateral boundary. We define the Rayleigh damping function  $\lambda(x)$  to be zero everywhere except in a narrow region near the boundary. Including this damping function alters the governing equations (2.7) and (2.11) to

$$u_t + F_x = -\lambda(x)(u - U), \quad (2.33)$$

$$\eta_t + K_x = -\lambda(x)\eta, \quad (2.34)$$

where  $F_x$  and  $K_x$  are the continuous fluxes corresponding to  $F_j^n$  and  $K_j^n$  above. Discretising these equations gives

$$u_j^{n+1} = u_j^{n-1} - \frac{dt}{dx} \left( F_{j+1}^n - F_{j-1}^n \right) - 2dt\lambda_j(u_j^{n+1} - U), \quad (2.35)$$

$$\eta_j^{n+1} = \eta_j^{n-1} - \frac{dt}{dx} \left( K_{j+1}^n - K_{j-1}^n \right) - 2dt\lambda_j\eta_j^{n+1}. \quad (2.36)$$

These are implicit equations which are usually solved using matrix inversion techniques. However, such complications do not arise here as (2.35) and (2.36) can easily be rearranged to give

$$u_j^{n+1} = \frac{1}{1 + 2dt\lambda_j} \left( u_j^{n-1} - \frac{dt}{dx} \left( F_{j+1}^n - F_{j-1}^n \right) + 2dtU\lambda_j \right), \quad (2.37)$$

$$\eta_j^{n+1} = \frac{1}{1 + 2dt\lambda_j} \left( \eta_j^{n-1} - \frac{dt}{dx} \left( K_{j+1}^n - K_{j-1}^n \right) \right). \quad (2.38)$$

Since we will be dealing with large amplitude waves it is likely that we will encounter problems due to nonlinear instability. This can be kept under control by including some form of artificial diffusion. In this program the diffusion process will be performed at the end of each timestep by simply averaging  $u^n$  and  $\eta^n$  according to the formula

$$q_j^n = \left( 1 - \frac{av}{2} \right) q_j^n + \frac{av}{4} \left( q_{j+1}^n + q_{j-1}^n \right). \quad (2.39)$$

### 2.3.2 Sensitivity to parameters

The Courant-Friedrichs-Levy condition states that we must have

$$dt < \frac{dx}{c}. \quad (2.40)$$

However, this condition only ensures stability for linear equations. Since we are solving nonlinear equations the condition on  $dt$  is more restrictive and it has been found, for the programs used in this study, that

$$dt < \frac{dx}{4c}. \quad (2.41)$$

Despite keeping  $dt$  small enough to ensure that the scheme remains stable, nonlinear instabilities still cause spurious oscillations in the solution. Instead of reducing  $dt$  further, which would result in longer run times, we introduce the  $av$  parameter described above. This smooths the solution and prevents the errors from building up. However, it can also reduce the maximum amplitudes of the waves. The optimum value of  $av$  is different in each situation depending on how close the mountain is to critical height. If  $h_{max}$  is sufficiently small for the linear approximation to be applicable,  $av$  can be set to zero, even though we are solving the nonlinear equations. However, as  $h_{max}$  is increased,  $av$  is progressively more important. We have considered each situation individually in this study and the results presented are those for which  $av$  is set to the minimum value for stability.

### 2.3.3 Results

To begin with we test the program against some results from Houghton and Kasahara (1968) who in turn have compared their results to the experiments of Long (1954). The obstacle shape is given by

$$h(x) = h_{max} \left( 1 - \frac{x^2}{a^2} \right), \quad (2.42)$$

where  $a$  is the half width and  $x$  is the distance from the centre of the obstacle. We run the program with the parameters

$$\bar{d} = 20 \text{ cm}, \quad (2.43)$$

$$h_{max} = 10 \text{ cm}, \quad (2.44)$$

$$a = 40 \text{ dx}, \quad (2.45)$$

$$dx = 1.0 \text{ cm}, \quad (2.46)$$

$$g = 980 \text{ cm s}^{-2}, \quad (2.47)$$

with 2000 gridpoints in the  $x$ -direction, as given by Houghton and Kasahara (1968), and  $dt = 0.0001$  s for stability, for several different Froude numbers. The results for  $F_0 = 0.2$  and  $F_0 = 1.9$  are given in figures 2.9 and 2.10 respectively. These figures are the same as the corresponding figures (14a and 14d) in

Houghton and Kasahara (1968). Houghton and Kasahara (1968) used a scheme developed by Lax and Wendroff which, unlike the Leapfrog scheme used here, is capable of handling shocks. Although we will not study flows containing shocks, it is interesting to see how the program copes with these situations. In fact, as shown in figures 2.11 and 2.12, it does surprisingly well. The general shape of the solution is as given in figures 14b and 14c of Houghton and Kasahara (1968) and the discontinuities are captured well with the exception of the upstream travelling jump in figure 2.11. Some oscillations are evident in the region of the discontinuities but this is to be expected - even the Lax-Wendroff code used in Houghton and Kasahara (1968) does this. The Leapfrog scheme remains stable by virtue of the averaging process explained in the previous section. With this switched off the program is unable to cope with the discontinuities and is soon outputting infinite values. The results in these four figures were produced with  $av$  set to 0.01. For values higher than this the solutions were considerably smoother with some discontinuities hardly apparent. For values lower than 0.01 the oscillations at the discontinuities were worse.

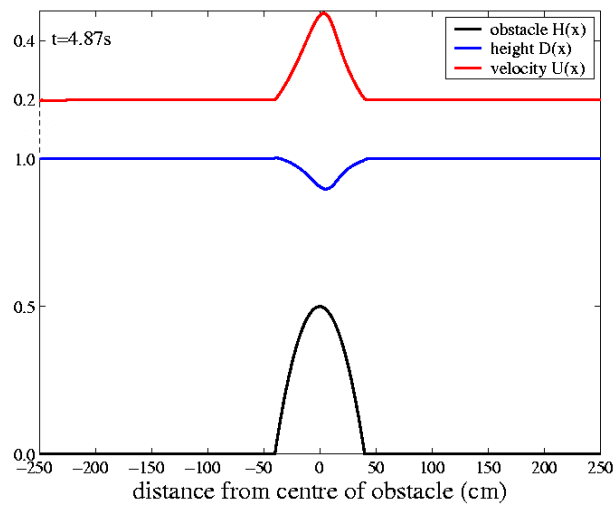


Figure 2.9:  $F_0 = 0.2$ . This figure corresponds to figure 14a in Houghton and Kasahara (1968). The height of the free surface (blue) and the velocity (red) are shown in the dimensionless units  $D = d/\bar{d}$  and  $U' = u/U$ . As expected, the free surface dips over the obstacle.

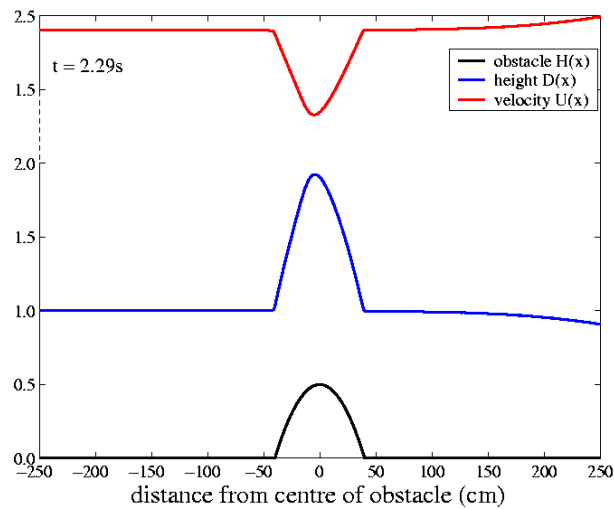


Figure 2.10:  $F_0 = 1.9$ . This figure corresponds to figure 14d in Houghton and Kasahara (1968). The height of the free surface (blue) and the velocity (red) are shown in the dimensionless units  $D = d/\bar{d}$  and  $U' = u/U$ . As expected, the free surface rises over the obstacle.

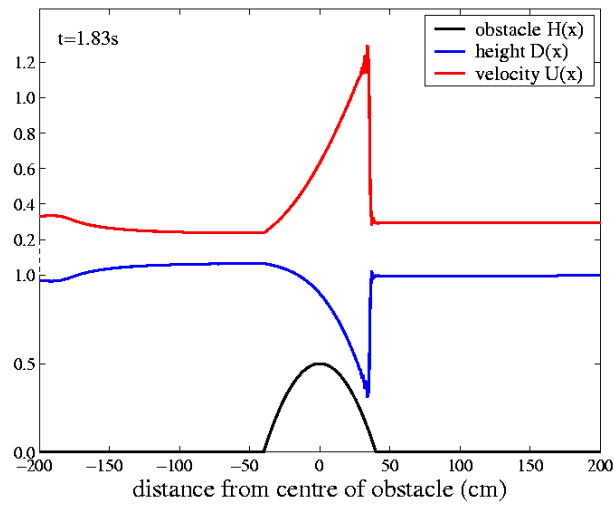


Figure 2.11:  $F_0 = 0.3$ . This figure corresponds to figure 14b in Houghton and Kasahara (1968). The height of the free surface (blue) and the velocity (red) are shown in the dimensionless units  $D = d/\bar{d}$  and  $U' = u/U$ . The maximum height of the obstacle is greater than the critical height so shocks form.

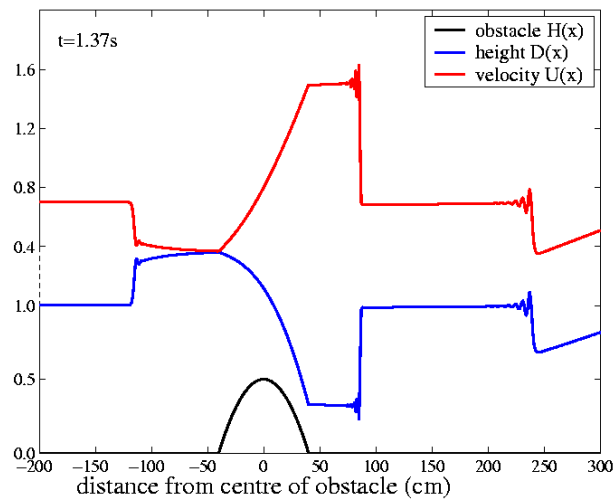


Figure 2.12:  $F_0 = 0.7$ . This figure corresponds to figure 14c in Houghton and Kasahara (1968). The height of the free surface (blue) and the velocity (red) are shown in the dimensionless units  $D = d/\bar{d}$  and  $U' = u/U$ . The maximum height of the obstacle is greater than the critical height so shocks form.

Having looked at the case where nonlinear effects are most important, we now turn our attention to the other extreme: the linear case. The following results are computed for length scales appropriate for the atmosphere rather than, as previously, for comparison with experiment. A scaled down version of the mountain has been included in each plot. The mountain scaling is the same in all three figures but the waves in figure 2.13 have been scaled up for clarity.

We can see from figure 2.13 that for a mountain of height  $h_{max} = 100m = 0.1\bar{d}$  the linear and nonlinear solutions are almost indistinguishable with particularly good agreement directly over the mountain. The nonlinear transient waves differ slightly from the linear solution, the maximum amplitude being more than and occurring behind that predicted by the linear theory. In figure 2.14 the mountain is sufficiently high for nonlinear effects to be apparent. The nonlinear solution develops a deeper dip over the mountain and the maximum amplitudes of the transient waves are even further behind the linear waves. In figure 2.15 the mountain has height  $h_{max} = 700m = 0.7\bar{d}$  which is 20m higher than the critical mountain height. The linear solution, as expected, gives no indication of the shock formation over the mountain. This feature is present in the nonlinear solution and it amplifies the effects of nonlinearity on the transient waves.

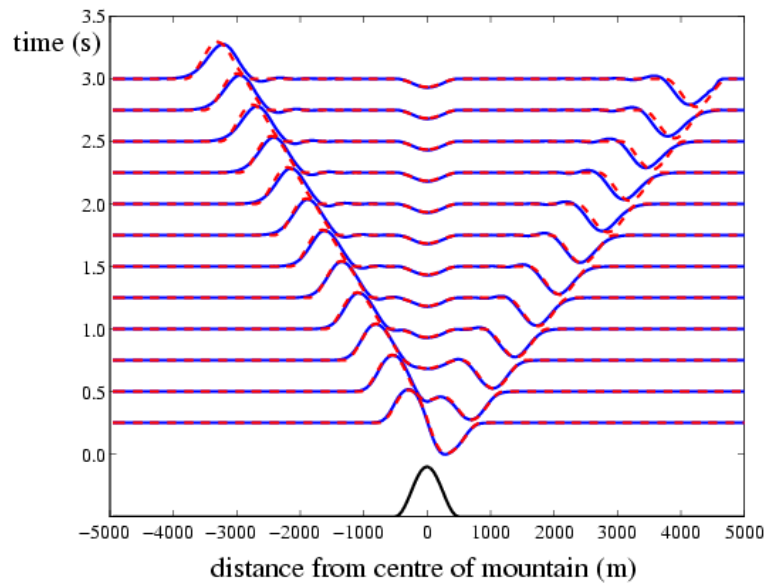


Figure 2.13: x-t diagram of the numerical solution (blue) compared to the exact linear solution (red) for the case where  $h_{max} \ll h_{crit}$

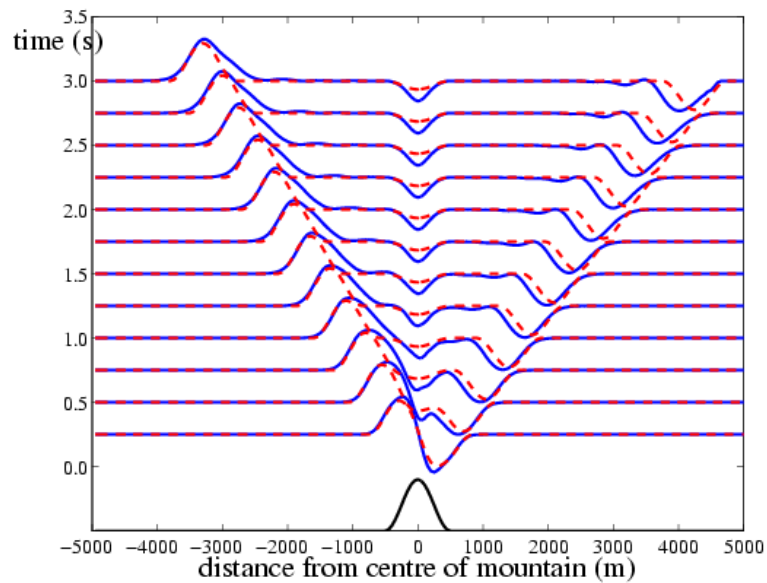


Figure 2.14: x-t diagram of the numerical solution (blue) compared to the exact linear solution (red) for the case where  $h_{max} < h_{crit}$

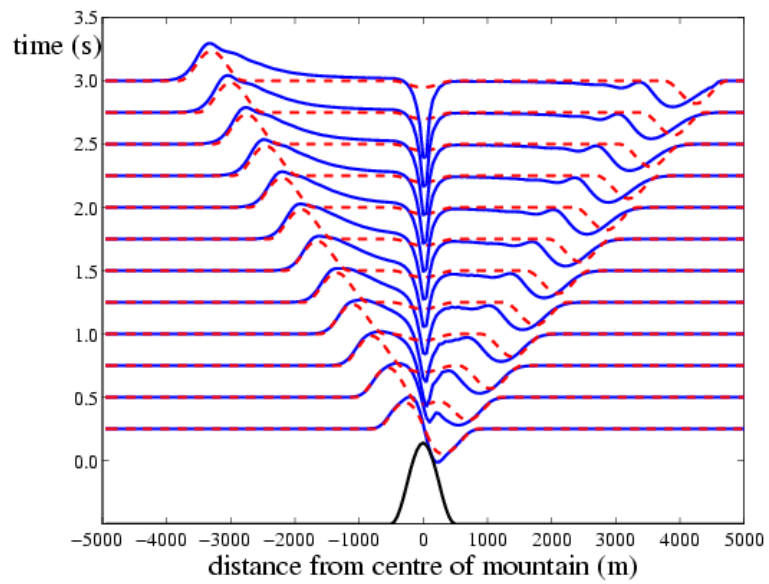


Figure 2.15:  $x$ - $t$  diagram of the numerical solution (blue) compared to the exact linear solution (red) for the case where  $h_{max} \sim h_{crit}$

# Chapter 3

## Stratified flow

So far we have only considered the flow in a homogeneous layer. In this section we examine the flow when the fluid is inhomogeneous, either due to a density stratification or a variation of wind speed with height. To begin with we investigate the theory of stratified flows. Much insight can be gained from the linear theory which we apply here to derive equations for the energy and momentum fluxes due to gravity waves.

### 3.1 Basic equations

If we make the incompressible approximation described in the introduction then

$$\frac{D\rho}{Dt} = 0. \quad (3.1)$$

Along with (2.1) and (2.2) this gives us a complete set of equations for the system. Taking the background flow to be  $(U, 0)$  and assuming a small disturbance we can set  $u(x, t) = U(z) + u'(x, t)$  and  $\rho = \rho_0(z) + \rho'(x, t)$  where  $U(z)$  and  $\rho_0(z)$  are the undisturbed values and  $u(x, t)$ ,  $\rho'(x, t)$  are small perturbations, and linearise

these equations to give:

$$\left(\frac{\partial}{\partial t} + U\frac{\partial}{\partial x}\right)u' + w'\frac{dU}{dz} = -\frac{1}{\rho_0}\frac{\partial p'}{\partial x}, \quad (3.2)$$

$$\left(\frac{\partial}{\partial t} + U\frac{\partial}{\partial x}\right)w' = -\frac{1}{\rho_0}\frac{\partial p'}{\partial z} - \frac{\rho'}{\rho_0}g, \quad (3.3)$$

$$\frac{\partial u'}{\partial x} + \frac{\partial w'}{\partial z} = 0, \quad (3.4)$$

$$\left(\frac{\partial}{\partial t} + U\frac{\partial}{\partial x}\right)\rho' + w'\frac{d\rho_0}{dz} = 0. \quad (3.5)$$

Taking the  $x$  derivative of (3.2) and substituting for  $\partial u/\partial x$  from (3.4) gives

$$\left(\frac{\partial}{\partial t} + U\frac{\partial}{\partial x}\right)\frac{\partial w'}{\partial z} - \frac{dU}{dz}\frac{\partial w'}{\partial x} = \frac{1}{\rho_0}\frac{\partial^2 p'}{\partial x^2}. \quad (3.6)$$

Eliminating  $\rho'$  from (3.3) using (3.5) leaves

$$\left(\frac{\partial}{\partial t} + U\frac{\partial}{\partial x}\right)^2 w' + N^2 w' = -\frac{1}{\rho_0}\left(\frac{\partial}{\partial t} + U\frac{\partial}{\partial x}\right)\frac{\partial p'}{\partial z}. \quad (3.7)$$

Adding  $\left(\frac{\partial}{\partial t} + U\frac{\partial}{\partial x}\right)\frac{\partial}{\partial z}$ (3.6) to  $\frac{\partial^2}{\partial x^2}$ (3.7), treating  $\rho_0$  as constant in (3.6), removes  $p'$ , leaving an equation for  $w'$ :

$$\left(\frac{\partial}{\partial t} + U\frac{\partial}{\partial x}\right)^2 \left(\frac{\partial^2}{\partial x^2} + \frac{\partial^2}{\partial z^2}\right)w' + N^2\frac{\partial^2 w'}{\partial x^2} - \frac{d^2 U}{dz^2}\left(\frac{\partial}{\partial t} + U\frac{\partial}{\partial x}\right)\frac{\partial w'}{\partial x} = 0. \quad (3.8)$$

By treating  $\rho_0$  as constant in (3.6) we have assumed that density variations are negligible compared to the other terms in the momentum equations but we have retained the density variation when it gives rise to a buoyancy force. This approximation is known as the Boussinesq approximation and it is applicable when the vertical scale of the motion is much less than the density scale height of the atmosphere (Nappo, 2002). If we assume that the motion is steady then this equation can be integrated twice with respect to  $x$ :

$$\frac{\partial^2 w}{\partial x^2} + \frac{\partial^2 w}{\partial z^2} + \left(\frac{N^2}{U^2} - \frac{1}{U}\frac{d^2 U}{dz^2}\right)w = 0. \quad (3.9)$$

Assuming a wave like solution of the form

$$w(x, z) = \hat{w}(z)e^{ikx}, \quad (3.10)$$

gives

$$\frac{\partial^2 \hat{w}}{\partial z^2} + \left( \frac{N^2}{U^2} - \frac{1}{U} \frac{d^2 U}{dz^2} - k^2 \right) \hat{w} = 0. \quad (3.11)$$

This has solution, for each  $k$ ,

$$\hat{w}(k, z) = \hat{w}(k, 0) e^{-imz}, \quad (3.12)$$

where

$$m = \left( \frac{N^2}{U^2} - \frac{1}{U} \frac{d^2 U}{dz^2} - k^2 \right)^{1/2}. \quad (3.13)$$

The sign of  $m$  has been chosen so that the energy propagates upward. To obtain a solution in physical space we take the inverse Fourier transform of (3.12).

Following Nappo (2002) this can be written as

$$w' = \int_0^{k_c} \hat{w}(k, 0) \sin(kx + mz) dk + \int_{k_c}^{\infty} \hat{w}(k, 0) e^{-qz} \sin(kx) dk, \quad (3.14)$$

where  $m = iq$  and  $k_c$  is the cut-off wave number, so called because waves with  $k < k_c$  are propagating whereas waves with  $k > k_c$  are evanescent. Therefore, the first integral gives the contribution to vertical velocity from propagating waves while the second gives the contribution from evanescent waves. From (3.11) we can see that the solutions will be propagating waves only if  $k^2 < L_s^2$  where  $L_s$  is defined by

$$L_s^2 = \frac{N^2}{U^2} - \frac{1}{U} \frac{d^2 U}{dz^2}. \quad (3.15)$$

This is the Scorer parameter referred to in the introduction.

## 3.2 Energetics

Gravity waves are important in the atmosphere because they transport energy. In this section we obtain an equation for the rate of change of perturbation energy, that is, the energy due to the perturbations to the constant background state.

Adding  $u'$ (3.2) to  $w'$ (3.3) we obtain

$$\frac{D}{Dt} \left( \rho_0 (u'^2 + w'^2) \right) + \rho' w' g = -u' \frac{\partial p'}{\partial x} - w' \frac{\partial p'}{\partial z} - \rho_0 u' w' \frac{dU}{dz}. \quad (3.16)$$

Using (3.4) we can write

$$u' \frac{\partial p'}{\partial x} + w' \frac{\partial p'}{\partial z} = \frac{\partial u' p'}{\partial x} + \frac{\partial w' p'}{\partial z}. \quad (3.17)$$

Substituting this into (3.16) gives

$$\frac{D}{Dt} \left( \rho_0 (u'^2 + w'^2) \right) + \rho' w' g = - \frac{\partial u' p'}{\partial x} - \frac{\partial w' p'}{\partial z} - \rho_0 u' w' \frac{dU}{dz}. \quad (3.18)$$

From (3.5) we see that

$$\rho' w' g = - \frac{\rho' g}{\rho_{0z}} \frac{D\rho'}{Dt} = \frac{g^2}{2\rho_0 N^2} \frac{D\rho'^2}{Dt}. \quad (3.19)$$

(3.19) then becomes

$$\frac{D}{Dt} \left( \rho_0 (u'^2 + w'^2) + \frac{g^2}{2\rho_0 N^2} \rho'^2 \right) = - \frac{\partial u' p'}{\partial x} - \frac{\partial w' p'}{\partial z} - \rho_0 u' w' \frac{dU}{dz}. \quad (3.20)$$

It is clear that

$$\frac{D}{Dt} \left( \rho_0 (u'^2 + w'^2) \right) \quad (3.21)$$

is the total rate of change of perturbation kinetic energy. It is not so clear that

$$\frac{D}{Dt} \left( \frac{g^2}{2\rho_0 N^2} \rho'^2 \right) \quad (3.22)$$

is the total rate of change of the perturbation potential energy. To see this we consider the gravitational potential energy  $PE$  gained by a fluid parcel when it is vertically displaced from its equilibrium position by a distance  $h$ . Denoting the buoyant force per unit volume by  $F_b$  we have

$$PE = - \int_0^h F_b dz \quad (3.23)$$

$$= - \int_0^h g \frac{d\rho_0}{dz} z dz \quad (3.24)$$

$$= - \frac{1}{2} \frac{d\rho_0}{dz} g h^2 \quad (3.25)$$

$$= - \frac{1}{2} \rho_0 N^2 h^2 \quad (3.26)$$

$$= \frac{1}{2} \frac{g^2}{\rho_0 N^2} \rho'^2, \quad (3.27)$$

where

$$\rho' = \rho_0(z) - \rho_0(z+h) \approx -h \frac{d\rho_0}{dz}. \quad (3.28)$$

So we have seen that the left hand side of (3.20) represents the total rate of change of the perturbation energy. Examining the right hand side of this equation shows us what this change is due to.  $u'p'$  and  $w'p'$  are the fluxes of wave energy in the horizontal and vertical directions respectively so the first two terms on the right hand side are the divergences of these fluxes. The final term is zero if there is no background wind shear and, if the buoyancy frequency is constant, wave perturbation energy is conserved.

### 3.3 Wind stress

Stress is the flux of momentum across a surface but care must be taken when discussing wave momentum. McIntyre (1981) deplores the use of language that perpetuates “the myth that waves possess momentum”. It is instead the flux of momentum, or wave stress, that is important. Following Nappo (2002) we multiply the steady, linearised horizontal momentum equation (3.2) by  $h(x)$  and integrate over  $x$  to get

$$\int_{-\infty}^{\infty} U h \frac{\partial u'}{\partial x} dx + \int_{-\infty}^{\infty} w' h \frac{dU}{dz} dx + \int_{-\infty}^{\infty} \frac{h}{\rho_0} \frac{\partial p'}{\partial x} dx = 0. \quad (3.29)$$

Using the linear boundary condition

$$w'(x, 0) = U \frac{dh}{dx}, \quad (3.30)$$

and noting that, for an isolated obstacle  $h(x) \rightarrow 0$  as  $x \rightarrow \pm\infty$ , we obtain

$$-\int_{-\infty}^{\infty} \rho_0 u' w' dx = \int_{-\infty}^{\infty} p' \frac{dh}{dx} dx. \quad (3.31)$$

This is Newton’s third law and it states that the drag per unit length exerted by the ridge on the flow is equal to the drag exerted by the flow on the ridge. We can define the wave stress over a length scale  $L$  to be

$$\tau(z) = -\frac{1}{L} \int_{-L/2}^{L/2} \rho_0 u' w' dx = -\rho_0 \overline{u' w'}. \quad (3.32)$$

### 3.4 Wave reflection, trapping and resonance

Atmospheric properties such as wind speed and buoyancy frequency change with height and if the change is sharp enough, such as at an inversion, vertically propagating waves may not be able to penetrate the layer and are instead reflected back down. In some cases the wave is only partially reflected, the rest of the wave being transmitted through the layer. Just as before this wave can be either propagating or evanescent. The lower layer now contains both upwards and downwards propagating waves and, depending on their wavelength and the height of the reflecting layer, they can either destructively or constructively interfere. Constructively interfering waves are trapped below the reflecting layer and are capable of transporting energy a considerable distance downstream. The continual generation of energy by the mountain can lead to resonance and this phenomenon explains the existence of strong downslope winds.

Typical vertical profiles of wind speed and buoyancy frequency in the atmosphere are complicated so for simplicity we consider the case of piecewise continuous Scorer parameter,  $L^2$ . This is a generalisation of the theory given in Gill (1982) and Nappo (2002) for piecewise continuous buoyancy frequency.

There are four possible forms of solution since we can have either propagating or evanescent waves in each layer. In the lower layer it is possible to have both upward propagating waves generated by the boundary and downward propagating waves reflected from the discontinuity in  $L^2$ . In the upper layer only waves propagating upward are possible. Thus

$$w' = A^{refr} e^{im_2(z-H)} e^{-i(kx-\omega t)}, z > H, \quad (3.33)$$

$$w' = \left( A^{in} e^{im_1(z-H)} + A^{refl} e^{-im_1(z-H)} \right) e^{i(kx-\omega t)}, 0 < z < H, \quad (3.34)$$

where  $A^{in}$  is the incident wave amplitude, and  $A^{refr}$ ,  $A^{refl}$  are the refracted and reflected wave amplitudes respectively. Since this is a linear analysis we apply the linearised form of the lower boundary condition (2.4) to find

$$w' = U \frac{\partial h}{\partial x} \frac{e^{im_1(z-H)} + r e^{-im_1(z-H)}}{e^{im_1 H} + r e^{-im_1 H}} e^{i(kx-\omega t)} \text{ for } 0 < z < H, \quad (3.35)$$

where we have defined the reflection coefficient  $r$  as the ratio of the amplitude of upward and downward propagating waves

$$r = \frac{A^{refl}}{A^{in}}. \quad (3.36)$$

We can find  $r$  by applying the conditions that the perturbation pressure  $p'$  and the vertical velocity  $w'$  are continuous across the interface. However, following Gill (1982) and Nappo (2002) this is simplified if we define the impedance  $Z = \frac{p'}{\rho_0 w'}$ . Since  $p'$  and  $w'$  are continuous across the interface,  $Z$  must also be. To calculate  $Z$  in each layer we must first calculate the perturbation pressure  $p'$ . To do this we assume wave like solutions of the form  $q'(x, z, t) = \tilde{q}(z)e^{i(kx - \omega t)}$  for each of the variables  $u'$ ,  $\rho'$ ,  $p'$  and  $w'$ . In this case equations (3.2) and (3.4) give

$$\tilde{p} = \frac{\rho_0}{k}((\omega - Uk)\tilde{u} + i\tilde{w}U_z), \quad (3.37)$$

$$\tilde{u} = \frac{i}{k}\tilde{w}_z, \quad (3.38)$$

which implies that

$$\tilde{p} = \frac{i\rho_0}{k^2}((\omega - Uk)\tilde{w}_z + i\tilde{w}U_z). \quad (3.39)$$

Using (3.35) and (3.34) we see that

$$\tilde{p}_1 = U \frac{\partial h}{\partial x} \left( B_1 e^{im_1(z-H)} + B_2 e^{-im_1(z-H)} \right) e^{-i(kx - \omega t)}, \quad (3.40)$$

$$\tilde{p}_2 = A^{refr} \left( \frac{\rho_0 m_2}{k^2} (\omega - Uk) - iU_z \right) e^{im_2(z-H)} e^{-i(kx - \omega t)}, \quad (3.41)$$

where

$$B_1 = \frac{\rho_0}{k^2} (\omega - Uk) m_1 + iU_z, \quad (3.42)$$

$$B_2 = \left( -\frac{\rho_0}{k^2} (\omega - Uk) m_1 + iU_z \right) r. \quad (3.43)$$

Returning to the analysis of Gill (1982) and Nappo (2002), we consider the case  $U_z = 0$ . Then these equations give the impedance in each layer as

$$Z_1 = \frac{m_1}{k^2} (\omega - Uk) \frac{e^{im_1(z-H)} - r e^{-im_1(z-H)}}{e^{im_1(z-H)} + r e^{-im_1(z-H)}}, \quad (3.44)$$

$$Z_2 = \frac{m_2}{k^2} (\omega - Uk). \quad (3.45)$$

Applying the condition that  $Z$  is continuous across the boundary gives

$$\frac{m_2}{m_1} = \frac{1 - r}{1 + r}. \quad (3.46)$$

Rearranging this as

$$r = \frac{m_1 - m_2}{m_1 + m_2} \quad (3.47)$$

gives us some information about the properties of the waves in each layer. By definition, if  $r = 0$  the wave will be propagating in both layers and  $m_1 = m_2$ . It is also clear from the definition of  $r$  that if  $|r| = 1$  there is total reflection and the wave is trapped in the bottom layer. If  $r = 1$  then  $m_2$  must be zero and the wave cannot propagate through the upper layer.

### 3.5 The hydrostatic approximation

In this section we examine the consequences of making the hydrostatic approximation. As we shall see in the next chapter, this approximation is essential for the formulation of the multilayer atmospheric model. Therefore we must understand the implications that the assumption of hydrostatic balance has on the flow.

The hydrostatic approximation imposes restrictions on the scale of flow to which the model can be applied. Following Gill (1982) we substitute (3.2) into the time derivative of (3.4) to obtain

$$\frac{\partial^2 w}{\partial z \partial t} = \frac{1}{\rho_0} \frac{\partial^2 p'}{\partial x^2}. \quad (3.48)$$

If we assume plane wave solutions this gives the relation

$$p' = -\frac{m}{k^2} \omega \rho_0 w_0 \cos(kx + mz - \omega t), \quad (3.49)$$

and (3.5) gives

$$\rho' = -\frac{N^2}{\omega g} \rho_0 w_0 \sin(kx + mz - \omega t). \quad (3.50)$$

Setting  $U = 0$  in (3.8) gives the dispersion relation

$$\omega^2 = \frac{N^2 k^2}{k^2 + m^2}, \quad (3.51)$$

which, along with equations (3.49) and (3.50), implies that

$$\frac{\partial p'}{\partial z} = -\frac{m^2}{k^2 + m^2} g \rho'. \quad (3.52)$$

Hence the hydrostatic approximation is valid only when  $k^2 \ll m^2$ , that is, when the horizontal scale of the motion is much larger than the vertical scale. Ironically, this result also shows that, for constant  $U$ ,  $m$  cannot vanish and the wave trapping discussed earlier will not occur. Thus, although the vertical scale of the motion is assumed to be small, hydrostatic theory produces vertical motion to a higher altitude than the non hydrostatic theory.

Partial reflection from a discontinuity in  $N$  is possible. This has been studied by Klemp and Lilly (1977) and we shall be comparing the model output to some of their results in section 4.3.2. It is may also be possible to produce reflection simply by varying  $U$  in such a way that  $d^2U/dz^2$  is non zero. This will be investigated in section 4.3.4.

# Chapter 4

## The multilayer model

In this chapter we return to the nonlinear theory. The atmosphere is approximated by a finite number of discrete homogeneous layers and the nonlinear equations are solved numerically within each layer. We will use this model to investigate some of the theory set out in Chapter 3.

### 4.1 Multilayer equations

We model the fluid as  $I$  incompressible, homogeneous layers and assume the interface between the layers to be infinitely thin. It is also assumed that no mixing occurs between the layers. Within each layer the flow is governed by the same equations as the single layer, namely

$$\frac{D\mathbf{u}_i}{Dt} = -\frac{1}{\rho_i}\nabla p_i - g\hat{\mathbf{z}}, \quad (4.1)$$

$$\nabla \cdot \mathbf{u}_i = 0, \quad (4.2)$$

where the  $i$  subscript labels the layer and the notation is the same as before, (see figure 4.1). The interaction between the layers occurs via the pressure term which can be found, as before, from the hydrostatic equation

$$-\frac{1}{\rho_i}p_{iz} - g = 0. \quad (4.3)$$

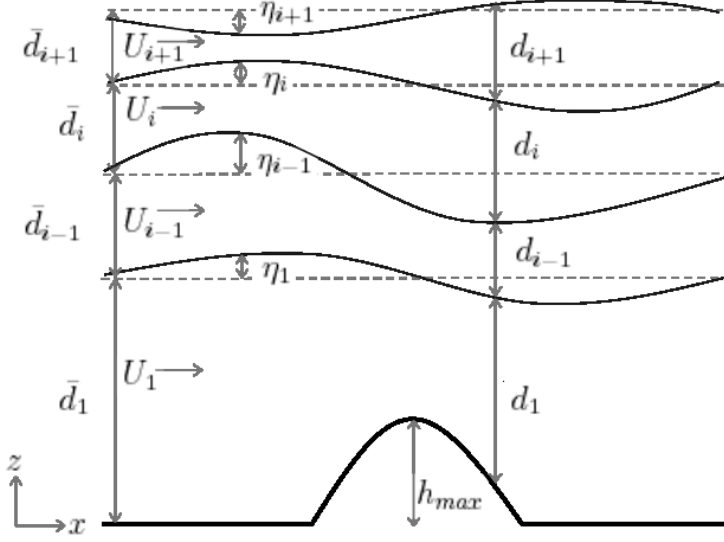


Figure 4.1: Definition diagram for the notation in the multilayer case.  $U_i$  and  $\bar{d}_i$  are respectively the upstream constant speed and depth in the  $i^{\text{th}}$  layer,  $\eta_i(x)$  is the displacement of the  $i^{\text{th}}$  interface and  $h(x)$  is the topography.  $d_i(x) = \bar{d}_i + \eta_i(x) - \eta_{i-1}(x)$  is the total depth of the  $i^{\text{th}}$  fluid layer.

Integrating this from a point  $z_i$  within the  $i^{\text{th}}$  layer to the top of the layer gives

$$p_i(z_i) = p_{is} + g\rho_i(z_{is} - z_i), \quad (4.4)$$

where  $p_{is}$  and  $z_{is}$  denote the pressure and height respectively at the surface of the  $i^{\text{th}}$  layer. For the top layer this is clearly

$$p_I(z_I) = p_s + g\rho_I \left( \sum_{j=1}^I (\bar{d}_j) + \eta_I - z_I \right) \quad (4.5)$$

where  $p_s$  is the pressure at the surface. For the  $I-1^{\text{th}}$  layer the equivalent equation is

$$p_{I-1}(z_{I-1}) = p_{(I-1)s} + g\rho_{I-1} \left( \sum_{j=1}^{I-1} \bar{d}_j + \eta_{I-1} - z_{I-1} \right). \quad (4.6)$$

If we impose the condition that the pressure is continuous across each interface so that

$$p_{is} = p_i \left( \sum_{j=1}^i \bar{d}_j + \eta_i \right) = p_{i+1} \left( \sum_{j=1}^i \bar{d}_j + \eta_i \right), \quad (4.7)$$

we can rewrite (4.6) as

$$p_{I-1}(z_{I-1}) = p_I \left( \sum_{j=1}^{I-1} \bar{d}_j + \eta_{I-1} \right) + g \rho_{I-1} \left( \sum_{j=1}^{I-1} \bar{d}_j + \eta_{I-1} - z_{I-1} \right). \quad (4.8)$$

Using (4.5) we see that

$$p_{I-1}(z_{I-1}) = p_s + g \left( \rho_I (\bar{d}_I + \eta_I - \eta_{I-1}) + \rho_{I-1} \left( \sum_{j=1}^{I-1} \bar{d}_j + \eta_{I-1} - z_{I-1} \right) \right). \quad (4.9)$$

Continuing this process we see that the general equation for the pressure in the  $i^{\text{th}}$  layer is

$$p_i(z_i) = p_s + g \left( \sum_{j=i+1}^I \rho_j (\bar{d}_j + \eta_j - \eta_{j-1}) + \rho_{I-1} \left( \sum_{j=1}^i \bar{d}_j + \eta_i - z_i \right) \right). \quad (4.10)$$

Substituting this into (4.1) and taking the surface pressure to be zero gives

$$u_{it} + u_i u_{ix} = -g \left( \frac{1}{\rho_i} \sum_{j=i+1}^I \rho_j (\eta_{jx} - \eta_{(j-1)x}) + \eta_{ix} \right). \quad (4.11)$$

Again we find the equation for  $\eta$  from the integrated form of the conservation equation:

$$0 = \int_{\Sigma_{j=1}^{i-1} \bar{d}_j + \eta_{i-1}}^{\Sigma_{j=1}^i \bar{d}_j + \eta_i} u_i dz - u_i \frac{\partial \eta_i}{\partial x} + u_i \frac{\partial \eta_{i-1}}{\partial x} + [w_i]_{\Sigma_{j=1}^{i-1} \bar{d}_j + \eta_{i-1}}^{\Sigma_{j=1}^i \bar{d}_j + \eta_i} \quad (4.12)$$

$$= \frac{\partial}{\partial t} (\eta_i - \eta_{i-1}) + \frac{\partial}{\partial x} (u_i (\bar{d}_i + \eta_i - \eta_{i-1})) \quad (4.13)$$

where we have applied the condition  $w_i = \frac{D\eta_i}{Dt}$  at each interface.

## 4.2 Multilayer program

The program `multilayer_program.f90` solves equations (4.11) and (4.13) using a similar process to that given in section 2.3.1, that is, the equations are solved using

a leapfrog scheme with a sponge layer to absorb the waves at the lateral boundary. The same process of numerical diffusion is also included. The only complication encountered in the multilayer case is the presence of an upper boundary. There is no such distinct upper boundary in the atmosphere. Therefore, we require an upper boundary condition that enables the waves to propagate out of the domain. This is accomplished by adding another sponge layer, this time to the top of the domain. The second damping function,  $\lambda_2(x)$  is plotted in green in figure 4.2. The discrete equations solved by this program are

$$u_{i,j}^{n+1} = \frac{u_{i,j}^{n-1} - \frac{dt}{dx}(F_{i,j+1}^n - F_{i,j-1}^n) + 2dt(\lambda_{i,j} + \lambda_{2,i,j})U_i}{1 + 2dt(\lambda_{2,i,j} + \lambda_{i,j})}, \quad (4.14)$$

$$\eta_{i,j}^{n+1} = \frac{\eta_{i,j}^{n-1} - \frac{dt}{dx}(K_{i,j+1}^n - K_{i,j-1}^n)}{1 + 2dt(\lambda_{2,i,j} + \lambda_{i,j})}. \quad (4.15)$$

As in the single layer case, we require some numerical diffusion to keep the scheme stable. This is accomplished in the same way as before.

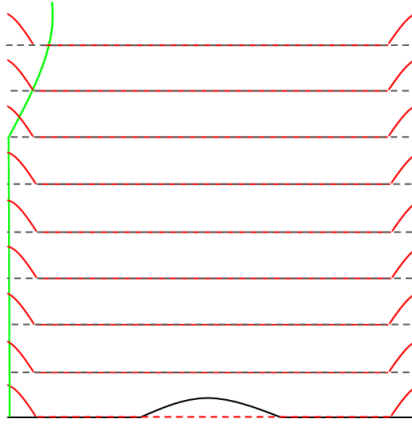


Figure 4.2: Diagram of the multilayer program. The undisturbed heights of the layers are shown in dashed grey, the topography is plotted in black. The damping functions are shown in red at the lateral boundary and in green at the upper boundary.

### 4.2.1 Sensitivity to parameters

The same conditions as outlined in section (2.3.2) apply to  $dt$  and  $av$  in this multilayer program. However, since we are now attempting to model a continuously stratified fluid by a set of discrete layers, we need to consider the vertical resolution, that is, the number of layers of constant density used to model a layer of constant buoyancy frequency. There has not been time to investigate this in depth. The number of layers in each simulation has been decided by a quick preliminary run.

When constructing the sponge layer at the upper boundary, care must be taken to ensure that it is deep and gently sloping. The depth ensures that the waves are fully absorbed while the gradual slope will prevent waves from reflecting. Again, the characteristics of the sponge layer are individual to each case.

## 4.3 Results

### 4.3.1 Two layer flow

In order to test the program we apply it to a simple situation, that of two superposed layers of different density. In this case equations (4.11) and (4.13) become

$$u_{1,t} + u_1 u_{1,x} = -g \left( \frac{\rho_2}{\rho_1} (\eta_{2,x} - \eta_{1,x}) + \eta_{1,x} \right) \quad (4.16)$$

$$u_{2,t} + u_2 u_{2,x} = -g \eta_{2,x} \quad (4.17)$$

$$\eta_{1,t} + (u_1 (\bar{d}_1 + \eta_1 - \eta_0))_x = 0 \quad (4.18)$$

$$\eta_{2,t} + (u_2 (\bar{d}_2 + \eta_2) + (u_1 - u_2) \eta_1 - u_1 (\bar{d}_1 + \eta_0))_x = 0 \quad (4.19)$$

Comparing the equations for  $u_1$  and  $\eta_1$  with those for flow in a single layer we see that there is only one additional term: the first term on the right hand side of (4.16). When we derived the single layer equations we stated that any fluid above the interface had negligible density and if we do neglect the density of the second layer by setting  $\rho_2 = 0$  we arrive at the single layer equations. Rewriting (4.16) as

$$u_{1t} + u_1 u_{1x} = -g \frac{\rho_2}{\rho_1} \eta_{2x} - g \left( 1 - \frac{\rho_2}{\rho_1} \right) \eta_{1x} \quad (4.20)$$

$$= -g \frac{\rho_2}{\rho_1} \eta_{2x} - g' \eta_{1x} \quad (4.21)$$

we see that if  $\eta_{2x}$  is relatively small, the motion in the lower layer is similar to that in a single layer with reduced gravity

$$g' = 1 - \frac{\rho_2}{\rho_1}. \quad (4.22)$$

If we make the rigid lid approximation  $\eta_{2x} = 0$ , the two cases become identical. This can be seen in figure 4.3.

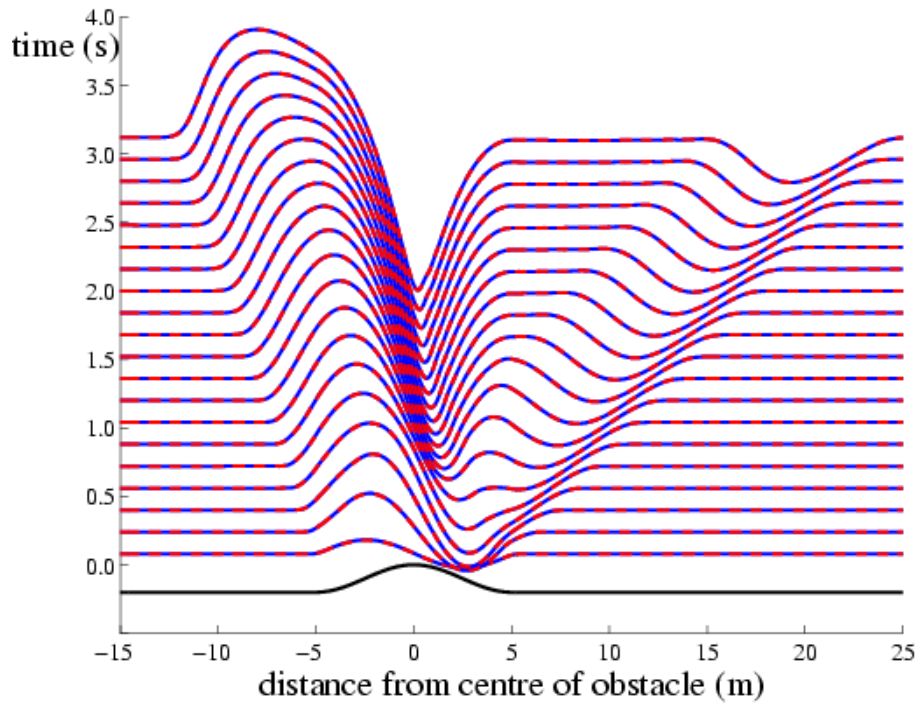


Figure 4.3: Two layer flow showing the solution for the lower layer (blue) compared to the solution for a single layer system with reduced gravity  $g'$ .

### 4.3.2 Partial reflection

Klemp and Lilly (1975) study a linear hydrostatic model of the atmosphere comprising three layers of buoyancy frequency. Their aim is to investigate the atmospheric conditions which produce intense surface winds. We aim to reproduce

their result (see figure 4.5) which shows partial reflection of the wave and a significant increase in wave amplitude in the lower layer. The values given in Klemp and Lilly (1975) for their three layers are

$$\begin{aligned} N_1 &= 1.6 \times 10^{-2} s^{-1}, & U_1 &= 15 m s^{-1}, \\ N_2 &= 0.9 \times 10^{-2} s^{-1}, & U_2 &= 25 m s^{-1}, \\ N_3 &= 2.0 \times 10^{-2} s^{-1}, & U_3 &= 45 m s^{-1}. \end{aligned}$$

For our model we need to construct these layers of buoyancy frequency out of layers of different density. Solving

$$\frac{\partial \rho}{\partial z} = -\frac{\rho}{g} N^2 \quad (4.23)$$

for  $\rho$  gives

$$\rho = e^{-N^2 z/g}. \quad (4.24)$$

Thus

$$\rho_i = e^{-N^2 z/g} \rho_{i-1}, \quad (4.25)$$

where the subscript  $i$  denotes the  $i^{th}$  layer. We can now build up the required  $N^2$  profile. We use 10 layers of density to each layer of buoyancy frequency. The result is given in figure 4.4. It shows good agreement with figure 4.5. The steep drop over the mountain is well produced but, although the disturbance persists to higher levels the shape is not quite correct - the surface rises a little before it drops and this feature is not present in Klemp's result.

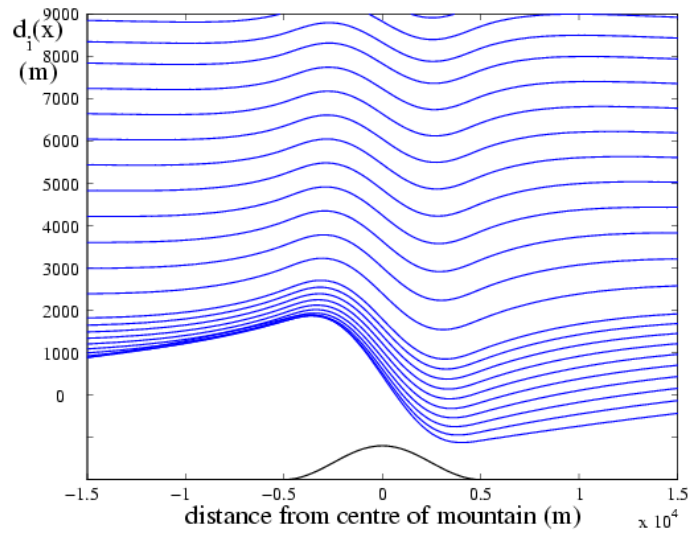


Figure 4.4: Numerical result from the multilayer model for the atmospheric profile detailed in equations (4.3.2),(4.3.2) and (4.3.2)

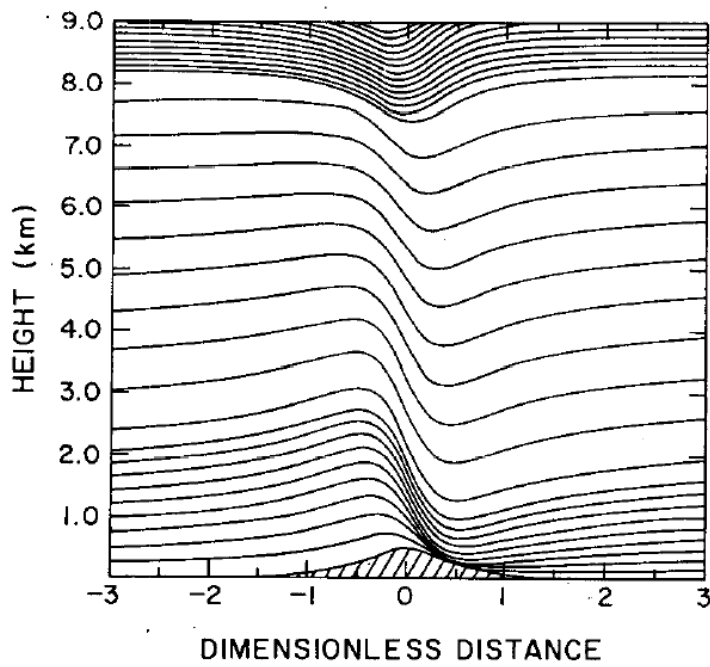


Figure 4.5: Linear streamline pattern for flow past a bell shaped mountain. From Klemp and Lilly (1975)

### 4.3.3 Variation of buoyancy frequency

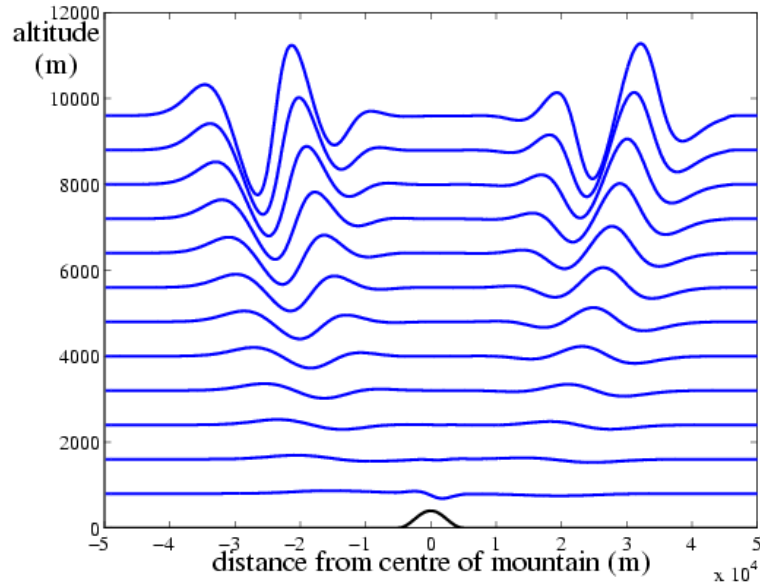


Figure 4.6:  $d_i(x)$  for  $m = 0.001m^{-1}$ .

Figures 4.6 and 4.7 show  $d_i(x)$  for two different values of  $m$ . The maximum amplitudes of the waves are greater in the case where  $m$  is smaller but this can be explained by the linear theory since the wave amplitudes are proportional to  $\frac{F_0}{2(F_0-1)}$  which is larger if  $U_0$  is. In order to investigate these differences further we plot the location of the maximum waves amplitues for both values of  $m$ , see figure 4.8. Again this is disappointing since there is little difference other than that which you would expect from a variation in wind speed.

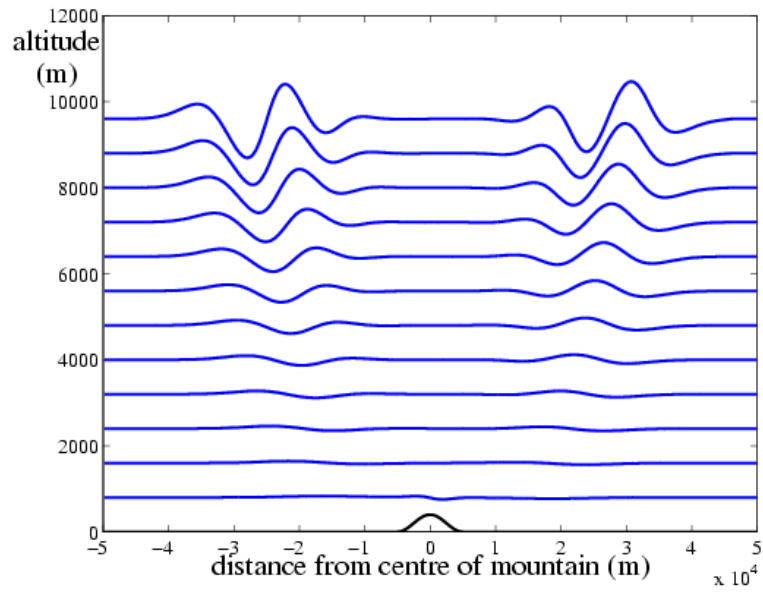


Figure 4.7:  $d_i(x)$  for  $m = 0.002m^{-1}$ .

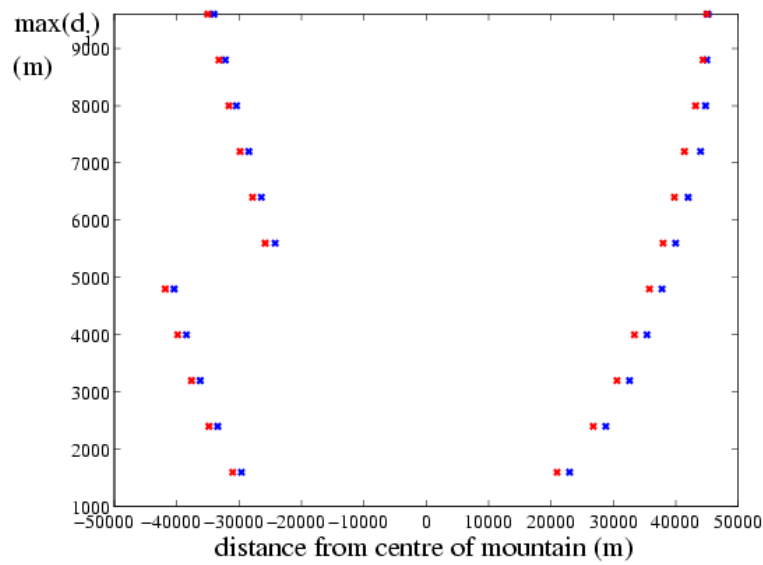


Figure 4.8: A comparison of the locations of the maximum wave amplitudes for  $m = 0.001m^{-1}$  (blue) and  $m = 0.002m^{-1}$  (red).

### 4.3.4 Vertical wind profile

In this section we investigate the effect of varying the initial wind speed with height as shown in figure 4.9.

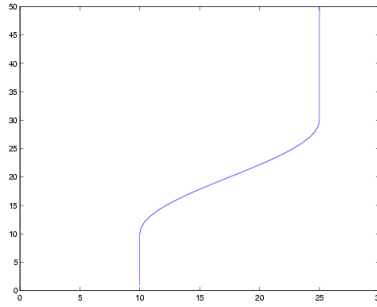


Figure 4.9: Initial vertical velocity profile,  $U(z)$ .

The results, shown in blue in figure 4.10, are not as expected. We were hoping to see some reflection at the layer where  $U$  is decreasing. The red curves show the result when the conditions are identical apart from the initial horizontal velocity which is a constant  $10\text{m.s}^{-1}$  for all  $z$ . There is some difference in the outputs above the critical layer, as is shown in figure 4.11, but it is believed that these differences are due purely to the different wind speed rather than to the fact that the waves have passed through a critical layer.

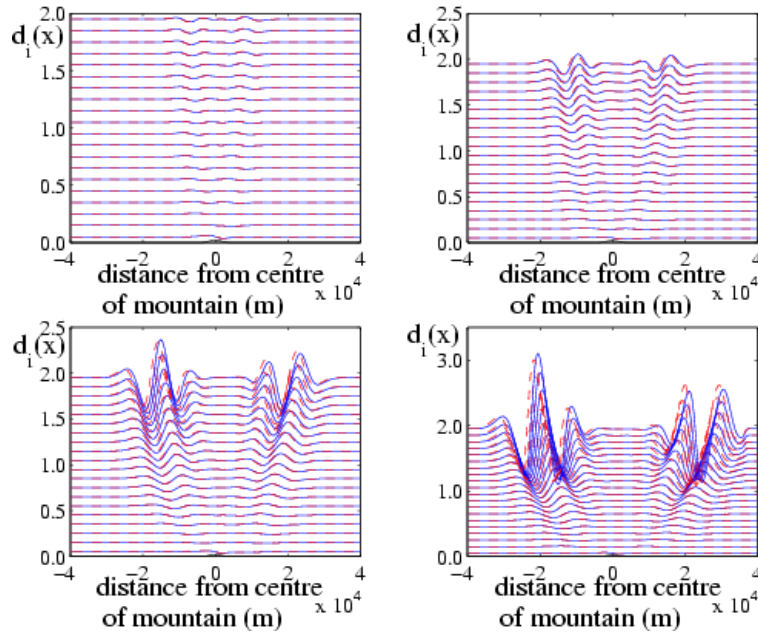


Figure 4.10: A comparison of  $d_i(x)$  in the case where  $U(z)$  is as given in figure 4.9 (blue), to the case where  $U = 10\text{m s}^{-1}$  is constant with height (red).

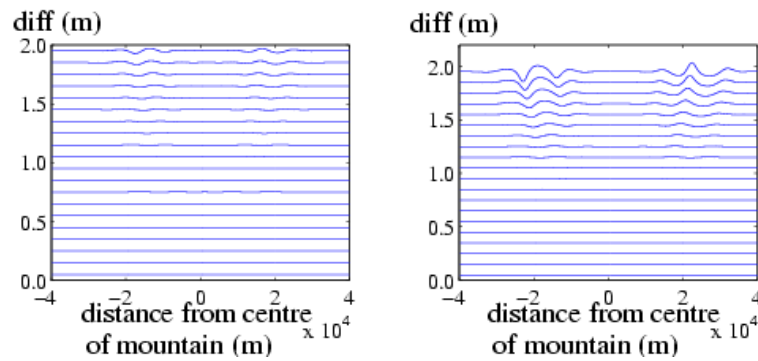


Figure 4.11: A plot of the difference between the two cases shown in figure 4.10, for the last two timeframes (before this there was little difference). As expected there is no difference below the critical layer but some difference above.

# Chapter 5

## Conclusions

This study has examined the importance of gravity waves in the atmosphere. The mechanism by which they are generated has been explained with particular emphasis on topographic forcing. The flow of a homogeneous layer over an isolated obstacle has been studied in detail and the numerical results agree well with those already established. The theory of stratified flow has been discussed and the numerical model extended to deal with multilayer, stratified flow. The results presented above have not been exactly as we envisaged and it is not clear that the multilayer system should exhibit the same characteristics as the continuously stratified flow it is attempting to represent.

### 5.1 Evaluation of the multilayer model

#### 5.1.1 Resolution

The horizontal resolution was set so that there were enough gridpoints in the  $x$  direction to represent the mountain. In the linear case the waves have wavelength equal to the width of the mountain so this resolution is sufficient. It is also adequate for the nonlinear cases considered in this study. In situations where shocks occur, greater resolution at the discontinuities would stave off instability but if these phenomena were to be studied in detail, an entirely different numerical method should be used.

The vertical resolution is of greater interest. In most cases the model has been run with all of the density layers having the same depth. The exception to this is the comparison with the Klemp and Lilly (1975) model where different layer depths were used in each of the levels of buoyancy frequency. Since this the case that produced the most encouraging results, it is likely that increasing the vertical resolution would have some positive effects. For example, Klemp and Lilly (1975) uses a vertical spacing based on the potential temperature. It may also be instructive to increase the resolution at critical layers. Perhaps the most obvious improvement would be to increase the depth of the first layer so that higher mountains could be modelled without losing resolution higher up in the atmosphere.

### **5.1.2 The sponge layer**

The necessary presence of a sponge layer at the upper boundary greatly increases the run time of the program. However, some way of approximating the condition that waves radiate outwards must be implemented. Durran (1999) suggests another option which involves including a viscous term in the upper layers but this does not necessarily improve the situation since a wave absorbing layer must still be implemented.

### **5.1.3 The hydrostatic approximation**

In the derivation of the equations of motion for a multilayer fluid we assumed the flow to be hydrostatic in order to find an expression for the pressure within each layer. However, it is possible to represent nonhydrostatic flow using a multilayer model simply by retaining the vertical velocity variable  $w$ .

## **5.2 Further work**

It is clear from the results presented in this study that more work is required before the multilayer model can be trusted to give reliable results. However, once the

model is workable, there are many other situations it can be applied to. These are outlined in the final sections below.

### 5.2.1 Layers with uniform density and vorticity

Following Baines (1995) we suggest that the layered model may better approximate a continuously stratified fluid if the velocity gradient, rather than the velocity, were uniform in each layer. Defining the mean velocity to be

$$U_i(z) = U(z_{(i-1)s}) + (z - z_{(i-1)s}) \frac{dU_i}{dz}, \quad (5.1)$$

where  $z_{is}$  is the undisturbed height of the top of the  $i_{th}$  layer, we see that this new approximation would give a continuous mean velocity profile. This is clearly a step closer to approximating a continuous velocity profile.

### 5.2.2 Rotational effects

Nappo (2002) makes the point that, since the hydrostatic approximation becomes more appropriate as the mountain width increases, there will come a point where the effects of the Earth's rotation will be felt. He calculates that a parcel travelling at  $10ms^{-1}$  will take 11 hours to cross a mountain range of width  $400km$  and on this timescale the Coriolis force will have an impact on the flow. Gill (1982) contends that, for large mountain chains, the slope will frequently change sign and it is the region in which the slope maintains the same sign that is important. In this case the length scale becomes  $10km$  and the nonrotating regime is again applicable. This justifies our neglect of the Coriolis force but it is obvious that there will be cases where it is important. It should be straightforward to adapt the program to include rotational effects.

### 5.2.3 Extension to more dimensions

For simplicity, this study has been limited to one dimensional flow over a two dimensional mountain. This gives an adequate indication of general properties

of the flow over a long ridge of constant cross section but even in this case it is evident that the ridge will end and the air will be able to flow around it. The characteristics of both two dimensional and fully three dimensional flow can be expected to be quite different from those of the simplified flow presented in this study.

# Bibliography

- J. R. Andrews, D. G. and Holton and C. B. Leovy. *Middle atmosphere dynamics*. Academic Press, 1987.
- P. G. Baines. *Topographic Effects in Stratified Flows*. Cambridge Univ. Press, 1995.
- G. A. Corby and C. E. Wallington. Airflow over mountains: the lee-wave amplitude. *Q. J. R. Meteorol. Soc.*, 82:266–274, 1956.
- D. R. Durran. *Numerical methods for wave equations in geophysical fluid dynamics*. Springer-Verlag, 1999.
- A. E. Gill. *Atmosphere-Ocean Dynamics*. Academic Press, 1982.
- D. D. Houghton and A. Kasahara. Nonlinear shallow fluid flow over an isolated ridge. *Comm. Pure Appl. Math.*, 21:1–23, 1968.
- J. B. Klemp and D. K. Lilly. The dynamics of wave induced downslope winds. *J. Atmos. Sci.*, 32:320–339, 1975.
- J. B. Klemp and D. K. Lilly. Numerical simulations of hydrostatic mountain waves. *J. Atmos. Sci.*, 35:78–107, 1977.
- R. R. Long. Some aspects of the flow of stratified fluids. 2. experiments with a two fluid system. *Tellus*, 6:97–115, 1954.
- M. E. McIntyre. On the “wave momentum” myth. *J. Fluid Mech.*, 106:331–347, 1981.

- C. J. Nappo. *Atmospheric Gravity Waves*. Academic Press, 2002.
- P. Queney. The problem of airflow over mountains: a summary of theoretical studies. *Bull. Amer. Met. Soc.*, 29:16–26, 1948.
- J. S. Sawyer. Numerical calculation of the displacement of a stratified airstream crossing a ridge of small height. *Q. J. R. Meteorol. Soc.*, 86:326–345, 1960.
- M. A. Scorer. Theory of waves in the lee of mountains. *Q. J. R. Meteorol. Soc.*, 75:41–56, 1949.